Multiple-instrument-based spectral irradiance of the Moon

Hugh H. Kieffer*
Celestial Reasonings, Genoa, Nevada, United States

Abstract. A model of lunar spectral irradiance incorporates data from multiple spacecraft and surface telescopic observations. Using 12 data sources derived from 90,000 lunar images, models that are smooth across both geometry and wavelength and involve only about 35 derived coefficients are found with a mean weighted residual of <0.5%. An irradiance libration model derived from lunar orbiter observations is used to reduce the number of coefficients required. Derivation uses iterative assignment of a single scaling factor for each band in each instrument, which is effectively the long-term lunar calibration coefficient for that band. Calibration of 26 instruments and two other published models reveals that although eight instruments agree within about 3% over 400 to 840 nm, some large biases exist. The model provides a sensitive assessment of instrument response trends. [DOI: 10.1117/1.JRS.16.038502]

Keywords: Moon; lunar; spectral; irradiance; calibration; model.

Paper 210833G received Dec. 22, 2021; accepted for publication Jul. 20, 2022; published online Aug. 13, 2022.

1 Introduction

Spacecraft instruments are calibrated in laboratory conditions against traceable standards, but their on-orbit response is often different and may continue to change for years. The Moon's surface is available to Earth-orbiters and is an extraordinarily stable diffuse reflector, 10^{-8} per annum.[1] However, what is needed for calibration is the spectral irradiance from this surface as illuminated by the Sun and viewed by spacecraft over a range of geometries, i.e., a lunar model. Lunar calibration,[2] which compares an instrument-reported irradiance of the Moon to the "actual" irradiance, has been based largely on the Robotic Lunar Observatory (ROLO) model,[3] or its later implementation by the Global Space-based Inter-Calibration System (GSICS) as GIRO.[4,5] The ROLO model, however, has several known issues. Its uncertainty is thought to be about 5%[6,7] or more [Ref. 8, Fig. 9(b)], the libration terms are constant over wavelength, and it requires 328 coefficients to generate results at 32 quite irregularly spaced wavelengths, which are then interpolated or convolved to the desired band. Conceptually, one could calibrate using radiance for a specific part of the Moon, but this is challenging due to the variegation of the Moon; radiance calibration has been used for lunar orbiters with ~100-m resolution.[9]

There have been several efforts to improve knowledge of lunar irradiance. Miller and Turner[10] developed a model to provide an estimate of lunar illumination of Earth scenes; however, it does not consider waxing/waning differences or libration. In a three-color mapping of lunar reflectance from 2593-m elevation based on calibration against the Sun, Velikodsky et al.[8] found the average ROLO albedo 13% lower than their observations. Wang et al.[11] have acquired lunar irradiance measurements over 400 to 1000 nm at a few phase angles with a calibrated imaging spectrometer from a high-altitude site; comparison indicates that the ROLO model is about 8% low. The lunar irradiance model of the European Space Agency (LIME) is based on six-band CIMEL observations from Tenerife.[12] At least three flight investigations are planned or active.[13]

The objective here of the spectral lunar irradiance model (SLIM) system is to utilize many data sources and a new methodology (SLIMED) to generate a significantly improved lunar

*Address all correspondence to Hugh H. Kieffer, HHKieffer@gmail.com

spectral irradiance model over the Solar-reflectance range, 350 to 2400 nm. Data for 25 instruments have been accumulated, more sources exist but were not available. From calibration using the ROLO model, it was known that gain differences were significant. Thus, the ability to apply an empirical gain to each instrument band is essential in combining many sources. Calibration by operating the resulting model allows an improved sensitivity and reliability in the measure of trends.

1.1 *Radiometric Nature of the Moon*

The Moon's surface has been in virtually the same environment since formation; the last major volcanic eruptions appear to have been in late Eratosthenian, ~1.2 billion years ago.[14,15] Its global photometric stability, based on cratering rates and the associated local albedo change, is 10^{-8} per annum.[1] The Moon appears gray to the eye, but its reflectance increases about a factor of 3 from 400 to 2500 nm. Its spectral reflectance is smooth apart from weak broad bands associated with FeO near 950 and 2000 nm.

In addition to the obvious change in brightness associated with the fractional illumination change through the month, the surface photometric function is near Lomell–Seeliger with a small mix of Lambertian. The albedo increases sharply at small phase angles, called "the opposition effect" associated with coherent back-scattering and shadow-hiding [Ref. 16, Chap. 9]. From the Earth, the study of the opposition effect is limited by onset of lunar eclipse near 1.6 deg but lunar orbiters can measure this to 0 deg. Using lunar reconnaissance orbiter data in a study of small phase angles, Velikodsky et al.[17] found that the width of the coherent-backscattering opposition effect ranges from 1.2 deg to 3.9 deg, dependent on wavelength and surface type. Thus, phase angle < ~4 deg remains a region to be avoided for calibration.

Lunar soil reflectance is weakly dependent upon temperature, <1% per 100 K relative reflectance, particularly near the FeO bands.[18] This is not treated explicitly in SLIM but is indirectly addressed through terms involving subsolar longitude and wavelength; the degree in wavelength would need to be five or more to isolate the FeO bands. Light reflected from the Moon is weakly polarized [Ref. 19, Fig. 8]. Lunar irradiance polarization is negative at small phase angle g, with a minimum $\sim -1.2\%$ near 10 deg, zero near $g \approx 25$ deg (wavelength dependent[20]), positive thereafter with a maximum beyond 90 deg of 6.6% (waxing), and 8.8% (waning). Modern measurements of the polarization of lunar light have been discussed extensively by Shkuratov et al.[21] The impact of lunar light polarization on calibration depends upon the polarization sensitivity of the instrument The ROLO and NIST telescopes were designed to be polarization insensitive, but spacecraft instruments can have significant polarization sensitivity, particularly those using scan mirrors. SLIM models do not currently consider polarization.

1.2 *Terminology*

For lunar modeling, the direction from the center of the Moon to the spacecraft vehicle or viewer is the sub-viewer selenographic longitude "Vlon" or x and latitude "Vlat" or y; together called "libration." The abbreviations and symbols are specific to this work. The direction to the Sun is expressed as the subsolar selenographic longitude "Hlon" or h and latitude "Hlat" or z. The key parameter is the signed phase angle p, this increases in time through a lunation, becoming positive discontinuously at full Moon. The absolute value of phase angle, g, is used in most equations, as is $q \equiv 1/g$. Wavelength λ, is usually shown in nanometers, however a value called "wave" or w based on micrometers, μm, is used in calculations.

2 Method and Materials

Within SLIM, all spectra are resampled onto a set of points starting at 300 nm and spaced by $\lambda/1000$, the last point is 2481.8 nm. For example, the reference solar spectrum $S_0(\lambda)$ (25,281 points, see Sec. 2.3), and the lunar albedo reference spectrum (LARS) $R_0(\lambda)$ (221 points, see Sec. 2.1) are put on this 2115 point system; their product times the geometric factor Ω/π is the lunar irradiance reference spectrum (LIRS), see Fig. 1. Ω is the solid angle of the Moon at

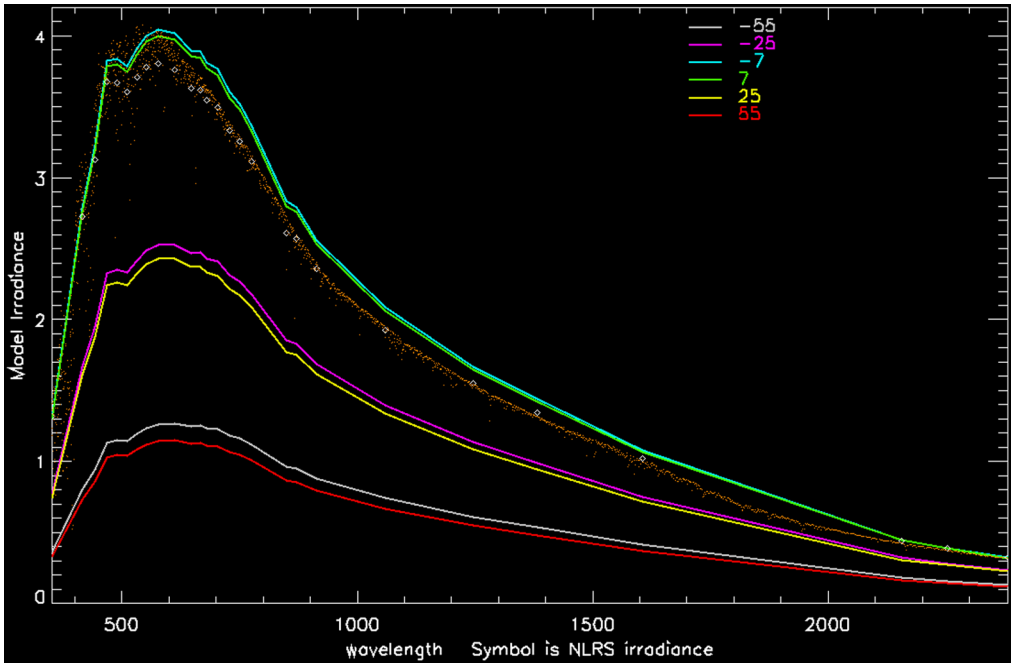

Fig. 1 The SLIMED Base model (see Sec. 4) at the effective wavelength of the 27 synthetic bands wavelengths (solid line), although the SLIMED models are continuous over wave. Phase angles 7 deg, 28 deg, and 55 deg are shown (color legend) for both waxing (negative) and waning Moon. Diamonds are the reference Moon at these wavelengths. Orange dots are the reference Moon on the SLIM uniform proportional resolution system, showing its full resolution.

standard distance, illuminated or not; $\Omega = 6.41780 \times 10^{-5}$ steradian. The system-level relative spectral response $T(\lambda)$ of each instrument band j is put on this point set and then combined with the LIRS to determine the equivalent width and the effective wavelength for the Moon

$$\lambda_{e_j} = \frac{\int_{\lambda_1}^{\lambda_2} \lambda \cdot S_0(\lambda) R_0(\lambda) T_j(\lambda) \mathrm{d}\lambda}{\int_{\lambda_1}^{\lambda_2} S_0(\lambda) R_0(\lambda) T_j(\lambda) \mathrm{d}\lambda}, \tag{1}$$

which is used throughout SLIMED models and calibration. The use of an effective wavelength is a rough approximation for panchromatic bands. Because of this, bands with an equivalent width/effective wavelength ratio of >0.2 are not used in model development. For calibration, wide bands can easily use a few weighted effective wavelengths spread across the band, which has not been done here. For practicality and to reduce noise, spectrometer data are averaged onto 27 flat-topped synthetic bands aligned with common spacecraft bands and intervening gaps.

2.1 *Theory*

The SLIMED model treats the effective spectral reflectance of the lunar disk $R(\lambda)$ viewed from the region of the Earth (out to geosynchronous orbit) as represented by $R_0(\lambda)$ multiplied by some continuous function of wavelength and photometric angles. The SLIM system allows a general dependence upon "wave" w, which may be wavelength in micrometers λ_1, or its inverse $\lambda_2 \equiv 1/\lambda_1$ or its natural log $\lambda_3 \equiv \ln \lambda_1$. Here, the log form is used unless explicitly stated otherwise.

Although the core of lunar models is lunar reflectance, the product is a lunar spectral irradiance E in the form

$$E_{\oslash}(\lambda) = S_{\odot}(\lambda, t) \frac{\Omega}{\pi D} \underbrace{R_0(P_0, \lambda) \mathbf{L}(P, w) \mathbf{B}(P, w)}_{\text{Disk Equivalent Reflectance}}. \tag{2}$$

Here, $S_{\odot}(\lambda, t)$ is the solar spectral irradiance at 1 astronomical unit (AU); this may be treated as constant or variable, as discussed in Sec. 2.3. D is the "distance factor" $d_V^2 d_H^2$, where d_V is the distance from the Moon's center to the viewer normalized to a standard distance of 384,400 km, near the mean Earth:Moon separation; and d_H is the Sun:Moon distance in AU. The distance factor used is based on $1/r^2$ irradiance, which ignores the small potential effect due to seeing less of the Moon when it is closer. Numerical simulation using the lunar orbiter laser altimeter (LOLA) map (Sec. 2.2) shows this approximation to be good at 0.044% for $g \leq 65$ deg.

The last three terms together constitute $R_{\oslash}(\lambda, P)$, the SLIM model of lunar disk-equivalent-reflectance (DER), which is a function of wavelength and photometric angles represented by P. Five angles, p, x, y, z, and h with four independencies, comprise P; only odd powers of h are allowed to avoid near-degeneracy with even powers of p. $R_0(\lambda)$ is the high-resolution nominal lunar reflection spectrum based on laboratory measurements of returned Apollo samples;[22–24] the 5% breccia mix used by ROLO[3] has been retained to make the LARS. Errors in the LARS that are higher in frequency than the wave polynomials will propagate into the mean calibration spectrum of each instrument.

L is a libration model (MapLib) derived here based on global lunar maps of spectral reflectivity made from observations by spacecraft orbiting the Moon, see Sec. 2.2. It has the form

$$L(P_i, w_j) = \sum_k d_k \underbrace{[1, p, p^2, p^3, p^4, p^5]\#[x, y, xy, z, x^2, y^2, xz, yz, xyz]}_{\mathcal{L}} + \sum_k d'_k w\mathcal{L}$$

$$\text{and} \quad \mathbf{L}(P_i, w_j) = \exp L(P_i, w_j), \tag{3}$$

where $\mathcal{L}$ represents the 54 cross-terms of the two sets in brackets. Any subset of the 108 terms can be selected to include in a fit, see Table 3. For increased numerical stability of the fit, all the independent variables are scaled to the order of 1; p is in radians, x and y are degrees/10 and z is in degrees. These maps were made at photometric geometries particular to each lunar mission and are quite different from the geometry of Earth-orbiting observations in avoiding the strong slope emphasis near the limb.

B carries the variation of the lunar irradiance over angles and wavelength in the form

$$B_{ij}(P_i, w_j) = \sum_{k=0}^{K} F_k(P_i) \underbrace{\sum_{m=0}^{M_k} c_{km} w_j^m}_{b_{jk}} \quad \text{and} \quad \mathbf{B}(P_i, w_j) = \exp B_{ij}(P_i, w_j), \tag{4}$$

where i is an observation index, j is a band index, k runs over the selected geometric basis functions (BF) F. The F_k terms involve the angles comprising P and some cross-products; each may be polynomials of low degree. M_k is the degree in wave for each of the k terms and c_{km} are the model coefficients. p and h are expressed in radians; x, y, and z are in degrees.

Model generation requires finding the coefficients c_{km} of **B** [Eq. (4)] for the least-squares best fit to the instrument observations adjusted to standard distances

$$E_{\oslash}(\lambda_j)_i = \underbrace{S_0(\lambda_j)\frac{\Omega}{\pi}R_0(P_0, \lambda_j)}_{\text{Ref. spectrum}} \underbrace{[1 + \mathcal{H}(\lambda_j, t_i)]}_{\text{Solar Variation}} \underbrace{\mathbf{L}(P_i, w_j)\mathbf{B}(P_i, w_j)}_{\text{Lunar Model}} G_j, \tag{5}$$

where t is the time of observation. Uncertainties are assigned to all measurements E_{ij}. Everything else is known except the empirical gains G_j, which are found from the residuals by iteration. Once G is incorporated, each instrument can contribute to filling in the sparsely populated illumination-observation geometry space. Once the **L** and **B** coefficients are known, Eq. (5) without the G term can be used to compute irradiances at standard distance for any observation; this is the SLIMED model. To adjust the desired total weight of an instrument, e.g., to avoid one instrument dominating a SLIMED model, a "heft" term is included, which multiplies all the weights $(1/\sigma^2)$ of an instrument.

Judgment choices include which instruments to use, the heft assignments, which geometric BFs to include, and the wave-degree for each. Empirical gains are initially set to unity and a set of three least-squares fits are done, rejecting points with residuals outside 3σ after each of the first two fits. The resulting mean weighted residual for each band is the basis for the gains applied for the next iteration, at the start of which the rejected points are reincluded.

A potential problem is finding the global minimum in a 168-dimensional space, the number of bands fit. To aid in this, the gain change at each iteration is limited based on a probability that is scaled to the average uncertainty of valid points for the band, typically significant only for the first iteration. For a band mean residual r, the change of ln gain is

$$\Delta = r\left[f_1 < 2\left(\left(1. - P\left(\frac{|r|}{U}\right)\right) < f_2\right].\right.$$

$P(x) \equiv \frac{1}{\sqrt{2\pi}}\int_{-\infty}^{x} e^{-t^2/2}\mathrm{d}t$ is the Gaussian probability function, [Ref. 25, Sec. 26.2.2]. The function between limit signs is a monotonic decreasing positive function near 1 for small r. f_2 provides a general damping factor on changes for all steps, initially 0.7; after three iterations, it is set to 0.9. f_1 is arbitrarily set at $\frac{1}{3}$. A large number of iterations is done to converge on the minimum.

2.2 *Libration Terms from Spacecraft Maps*

High-resolution simple-cylindrical maps of the Moon at several wavelengths have been derived from spacecraft orbiting the Moon and can be used to derive a libration model. The Clementine UV-VIS imager has bands at 415, 700, 600, 950, and 1000 nm and the maps are pole-to-pole. The NIR imager has bands at 1000, 1250, 1500, 2000, 2600, and 2780, the maps cover ± 70 deg. These maps[26] have increasing shadows toward the poles. Gores constitute <1% in these maps and tend to elongate in latitude; they were filled by linear interpolation along line. The maps were then resampled by averaging to 8 pixel/deg resolution. Clementine map longitude averages start to increase beyond 56 deg from the equator and become noisy starting near 75 deg. The 2600- and 2780-nm bands are distinctly different, may be influenced by thermal radiation, and were not included in the libration fits. For irradiance analysis, Clementine maps pole-ward of 69 deg were set to be uniform with the average over both hemispheres over 64 deg: 69 deg; this represents ~6.6% of the disk.

The LOLA returned signal strength at 1084 nm was converted into a surface zenith, zero-phase, albedo map with global coverage at 8 pixels/deg.[27,28] Contrast related to topography is typically small near zero phase; applying LOLA to Earth-view libration assumes that the local relation of the reflectance of slopes (particularly equator-ward) to reflectance of adjacent flat terrain is reasonably consistent over the near-side.

A study of possible libration angles for geocentric [as surrogate for low earth orbit (LEO)] and geosynchronous Earth orbit (GEO) locations indicated that a grid extending to ± 8 deg in Vlat and Vlon (± 12 deg for GEO) would cover nearly all possibilities. The irradiance using the 8 pixel/deg maps was computed for a "GEO" geometric grid covering this range with 4-deg spacing, Hlat ± 1.5 deg, and phase $\pm[3, 8, 14, 20, 30, 40, 50, 60, 70, 80, 90]$ deg for a total of 1540 points for each band. The subsolar longitude (Hlon) is computed to strictly maintain phase angle; points where the phase angle is smaller than the difference between viewer and solar latitude are not used.

The simple and colorless Lomell–Seeliger photometric function, $\mathcal{P} = \frac{\mu_0}{\mu_0+\mu}$, was used to compute the reflected radiance at each map point, μ_0 and μ are cosine of the incidence and emergence angles. The Lunar–Lambert photometric relation was tried for $\mathcal{P}$, this has a proportion of Lambertian reflectance that increases with g.[29,30] The fractional difference in the resulting normalized irradiance between these two functions is small, for g up to 60 deg, the mean difference is 0.018% with StdDev is 0.19%, the extreme of 1.5% is at large negative phase and Vlat. More recent photometric relations are available[31–33] but these involve 448 to 2172 coefficients. Some derivation of these complex relations may be useful for later versions of SLIMED.

Fig. 2 The Moon as it would appear at phase of −45 with libration of 8 deg E, 4 deg S. 8 pixel/ deg simple-cylindrical map of LOLA albedo reprojected to 700 pixel diameter.

Irradiance is linear with the summation over the map where both illuminated and visible

$$E = \sum_j \cos\,\theta_j \sum_i (\mu_{ij} > 0) A_{ij} \mathcal{P}_{ij}(\mu_0, \mu, g), \tag{6}$$

where i is the sample, j is the line, θ is the map latitude, and A is the mapped reflectance. This result is equivalent to summing over an orthographic projection for the same illumination and viewing geometry, an example image is Fig. 2. The irradiances for each phase are normalized to the $(x, y, z) = (0,0,0)$ libration point. The libration effect is about 2% except near the waning half-Moon where it reaches 6% for the lowest Vlon. The Moon is on average about 0.35% dimmer at the northern subsolar limit than at the southern limit.

2.3 *Solar Spectral Irradiance and Its Variation*

The 0.025-nm resolution version of the TSIS-1 hybrid solar reference spectrum (HSRS)[34] was used as $S_0(\lambda)$, the constant solar spectrum. Variation of both total and spectral solar irradiance are small but well-known. Total solar irradiance (TSI) $H(t)$ has been measured with a precision of about 1/10,000 over the period of lunar observations considered here. The TSI measurements from several sources were merged onto a consensus scale covering November 17, 1978, to December 31, 2015, by de Wit et al.[35] This dataset was extended using the same methodology to May 15, 2019, by Kopp[36] and here further extended to February 16, 2021, using TSIS data[37,38] and adjusting for the small bias in the time overlap with the consensus record. Over this 42.3-year daily record, the standard deviation (StDev) is 0.36 ppt, the range is $-2.87 : +1.58$ ppt, and the fraction of time the magnitude exceeds 1 ppt is 1.1%. The relative variation with wavelength is based on a quadratic fit in log/log space over 290:2412 nm to the ratio f of solar spectral irradiance variation (high-pass filtered) to TSI variation provided by Kopp, yielding

$$f(\lambda) = \exp(-0.338752 - 0.785894\,\ln\,\lambda + 0.202152(\ln\,\lambda)^2), \tag{7}$$

where λ is in micrometers; the mean weighted absolute residual is 2% of the mean weighted value. Solar variation is implemented in SLIM as

$$S_{\odot}(t,\lambda) = S_0(\lambda)\left[1 + \underbrace{f(\lambda)\left(\frac{H(t)}{H_0} - 1\right)}_{\mathcal{H}}\right], \tag{8}$$

where $S(t,\lambda)$ is the solar spectral irradiance and H_0 is the average of $H(t)$ over the dataset, $1361.62\,\mathrm{W/m^2}$. $\mathcal{H}(t,\lambda)$ is the solar variation model. It can optionally be applied to the irradiances going into a model fit and/or a calibration, normally both.

2.4 *Available Lunar Irradiance Observations*

With the exception of the NIST surface observations,[39] all lunar observation data were supplied by representatives of the instrument teams, see Table 1 and Table 8 in Appendix C. Teams provide the time of observation, location of the instrument at that time, and the measured spectral irradiance in each band. The time and location are converted into distances and angles using the JPL DE430 ephemeris.[40] Relative spectral response data are largely from instrument websites. Although team assessment of uncertainties is desirable, these were rarely provided. Some supplied datasets have points that are clearly outliers in calibration; these points are assigned huge uncertainties. LEO instruments usually point at or near geocentric nadir and require something special to view the Moon, commonly an attitude maneuver to point at the Moon, or use of a scan mirror at an unusual angle, or some combination of these. GEO instruments observe the Moon off the limb of the Earth in their field of regard as part of normal operations; some have special sequences to track the Moon. More details are in Appendix A.

2.5 *Photometric Geometry*

Of the five photometric angles used in the irradiance model, phase angle has by far the major effect on irradiance; there is a few percent difference between waxing (−) and waning (+) phases. Strictly, there are only four independent geometric variables. With the addition of wavelength, there are six dimensions, making display challenging. Generally, Hlon is close to the negative phase, and Hlat has a small range ±1.6 deg, leaving three prime geometric dimensions, plus wavelength.

The nine LEO instruments and three observatory instruments used in SLIMED fits are listed in Table 2. Coverage of these three angles for the spacecraft instruments is shown versus the cumulative time index in Fig. 3. Each instrument has a limited phase range except ROLO, AeroNet, and both PLEIADES. For these four, the distribution in libration is similar and generally well spread in both axes apart from PLEIADES concentrations near ±40 deg. SeaWiFS is largely near ±7 deg, with a few spread out at larger phases of both signs. OLI is largely near +8 deg, with a few negative. Moderate-resolution imaging spectroradiometer (MODIS) are largely near 55 deg with one-fourth to one-third spread out to 80 deg; Terra are all positive and Aqua are all negative. Both VIIRS are all near −50 deg. Both PLEIADES are spread over ±100 deg with concentrations at ±40 deg.

3 Data and Parameter Selection

The geometric BFs available in SLIM are listed below, these are the same as for the ROLO model.[3] Each of these (except constant) can independently be made polynomial and each of those may independently be multiplied by a polynomial in wave to generate the full set of SLIMED BFs

constant: 1

phase: g, absolute phase angle in radians, polynomial;

1/g: $1/g$, inverse absolute phase angle in radians, polynomial;

Hlon: h, subsolar longitude in radians; polynomial of odd powers;

Hlat: z, subsolar latitude in degrees; polynomial (only first degree used);

Vlon and Vlat: x, y, subviewer longitude and latitude in degrees; polynomial, same degree for both;

Table 1 Available data, grouped by type. "Band" is the number of useful bands, "Lun" is the number of distinct lunations covered; "Time" is the number of observation times, "Points" is the number of observations points with useful uncertainty. The three phase-angle columns are the minimum, the smallest absolute, and the maximum. The last column is the percent of observations before full-Moon. ROLOG is ROLO 311-g dataset. AerN is AeroNet on Mauna Loa. Description in Appendix A.

		Number of				Phase			%
Instrument	Acronym	Band	Lun	Times	Points	Min	Abs	Max	Wax
LEO	—	—	—	—	—	LEO	—	—	—
SeaWIFS	SeaW	8	144	204	1632	−48.9	5.1	65.5	57
EO1-Hyperion	HypM	26	18	20	520	−28.3	6.9	29.4	15
Terra-MODIS	MODT	20	192	993	19,798	47.9	47.9	81.5	0
Aqua-MODIS	MODA	19	175	743	14,117	−79.9	36.9	−36.9	100
Suomi-VIIRS	VIIRS	14	70	71	966	−56.2	49.8	−49.8	100
NOAA20-VIIRS	VIIRN	14	28	28	387	−52.0	50.1	−50.1	100
Landsat-8	OLI	9	70	1080	9720	−8.4	5.4	9.7	3
PLEIADES-A	PleA	5	61	141	698	−94.5	2.1	111.9	47
PLEIADES-B	PleB	5	42	339	1669	−101.5	1.4	101.6	50
GEO	—	—	—	—	—	GEO	—	—	—
GOES-8	GS8	1	38	44	44	−91.1	4.3	84.1	43
GOES-9	GS9	1	7	9	9	−70.4	10.0	82.5	56
GOES-10	GS10	1	40	49	49	−89.3	7.3	89.6	53
GOES-11	GS11	1	49	77	77	−87.6	4.5	89.9	61
GOES-12	GS12	1	38	49	49	−83.4	6.8	66.5	51
GOES-13	GS13	1	26	47	47	−76.9	6.4	74.3	53
GOES-15	GS15	1	14	28	28	−52.8	2.6	69.0	57
MSG-1-SEVIRI	SEV1	4	183	1190	3669	−153.0	1.5	156.1	52
MSG-2-SEVIRI	SEV2	4	162	1313	3645	−158.1	1.3	158.7	50
MSG-3-SEVIRI	SEV3	4	82	630	1744	−155.7	1.6	157.2	51
MSG-4-SEVIRI	SEV4	4	31	225	655	−155.4	3.6	147.6	52
GOES-16-ABI	ABI16	6	15	115	690	−76.0	5.6	69.9	58
GOES-17-ABI	ABI17	6	15	121	726	−73.6	5.0	72.3	57
Other	—	—	—	—	—	Other	—	—	—
Obs. @2148 m	ROLOG	32	30	1249	39,007	−124.7	1.4	109.3	39
Obs. @2367 m	NIST	9	1	2	18	19.8	19.8	19.8	0
Obs. @3402 m	AerN	7	20	50	350	−73.9	4.3	86.8	52
HiRISE-Mars	HiRIS	3	1	4	12	69.6	69.6	69.6	0

Table 2 Uncertainties, heft and net weights for the instruments fit by SLIMED. The first three columns apply to all models and list the instrument acronym, how many observations were made and the nominal uncertainty assigned to the instrument. The central columns list the "Heft" assigned and the right five columns lists the resulting percentage weight each instrument contributed to the final fit; "Hu" is uniform weight for each instrument, "H1" is all heft equal 1, and "Bal" includes only instruments that are roughly balanced between waxing and waning phases. ∼B is the Base model rounded for clarity.

			Heft			Total weight				
Inst acro	Num. times	Ave. Uncert.	Base	Hu	bal	∼B	Base	Hu	H1	bal
SeaW	1632	0.030	1.644	2.10	1.64	10	9.99	8.45	4.02	8.78
HypM	520	0.100	5.936	73.0		1	1.00	8.12	0.11	
MODT	19,860	0.050	0.379	0.48	0.38	10	9.96	8.36	17.38	14.78
MODA	14,117	0.050	0.432	0.69	0.43	8	7.95	8.42	12.09	11.98
VIIRS	994	0.050	3.856	9.70		5	4.99	8.32	0.86	
VIIRN	392	0.050	19.250	24.0		10	9.98	8.25	0.34	
OLI	9720	0.030	0.310	0.39		10	9.97	8.34	21.30	
PleA	705	0.050	10.974	17.3	10.97	8	7.99	8.34	0.48	15.19
PleB	1695	0.050	4.777	7.60	4.78	8	7.99	8.42	1.10	15.90
ROLOG	39,968	0.050	0.335	0.21	0.34	20	20.0	8.34	39.53	28.79
NIST	18	0.006	1.722	4.30		5	4.99	8.26	1.92	
AerN	350	0.030	4.000	9.70	4.0	5	5.21	8.38	0.86	4.58

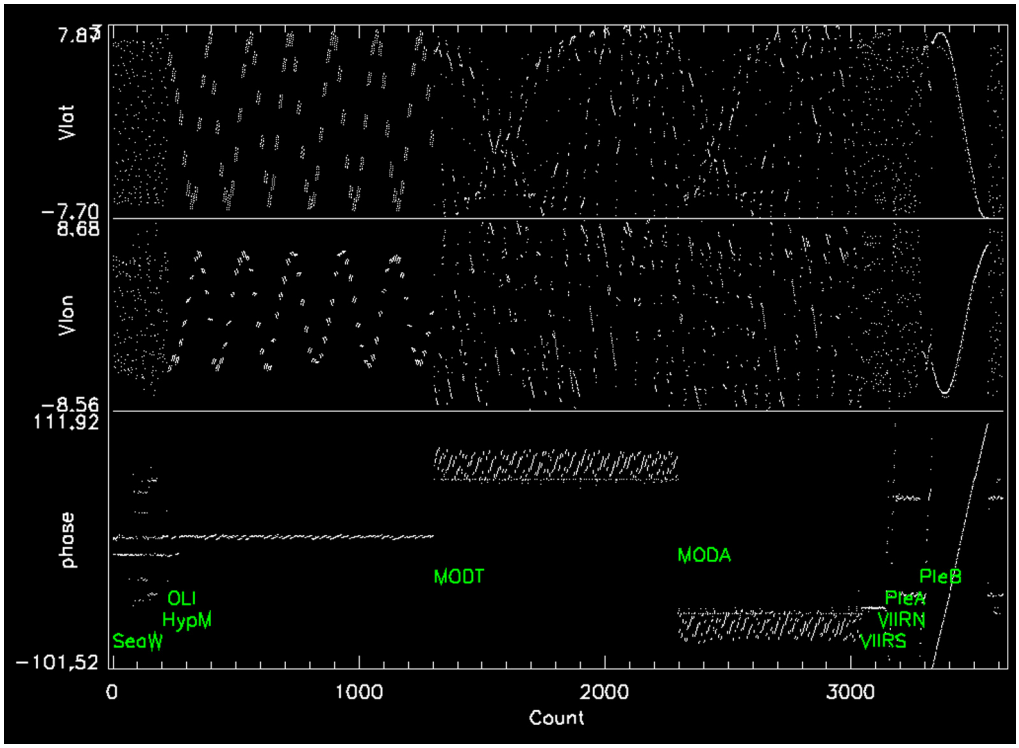

Fig. 3 Geometry coverage over cumulative time index for the nine spacecraft instruments used in SLIMED fits. Each angle and its range are shown at the left. Data for each instrument begins at the abscissa of the left edge of its acronym (in green). PleB did a dense sweep in phase angle covering the bright half of a single lunation.

hx and *hy*, subsolar longitude (radians) times subviewer longitude or latitude (degrees); polynomial, same degree for both.

Several other terms used in the ROLO model are available; these are all nonlinear, involve additional fitting loops, and were rarely used in SLIM development. Because the goal is a calibration model, the absolute phase angle in SLIMED fits here is restricted to $3 \leq g \leq 95$ deg, and terms addressing the opposition effect are less important.

All three wave modes were tried. The effect of wave-mode is most easily seen as the variation of the sum of the BFs with wavelength, b_{jk} in Eq. (4). In SLIMED models, this term has a relatively low value at extreme wavelengths. This drop is greatest at short wavelengths for $w = \lambda$ and at long wavelengths for $w = 1/\lambda$. This led to adopting $w = \ln \lambda$ for the Base model (Sec. 4).

Starting with all gains equal unity, after 19 iterations the largest change of gain was 0.076%, the average was 0.023%; see Fig. 13. With the c_{km} determined, the model irradiance E_m for any wavelength and geometry can be calculated, applying MapLib and solar variation consistent with model generation. The lunar calibration ratio is $R_C = E_d/E_m$ where E_d is the irradiance reported by the team, adjusted to standard distance; optionally, the current trend model (Sec. 3.1) for a band can be applied to E_d. The weighted average over date of R_C for a band is its empirical gain.

Differences between SLIMED models or other published models were assessed using the GEO geometry grid, Sec. 2.2. For wavelength, the eight bands chosen by the GSICS lunar calibration group were used: centered on 442, 550, 670, 765, 870, 1380, 1640, and 2350 nm and with trapezoidal response, 10-nm wide at top and 30-nm wide at zero response.

Estimates of many potential errors in lunar calibration are listed in Appendix B. The values are generally not precise, but their magnitude indicates areas that need effort. Any bias in radiometric calibration that is systematic across the data sources would propagate invisibly into the model.

3.1 *Trends*

Changes in instrument gain over time are usually decreasing and continuous. Smooth fits to gain changes are called "trends." Derivation of gain trends in SLIM is based on calibration ratios and are not normalized. However, in application, trends are normalized to their values at the first lunar observation for that instrument, separating the empirical gain from the trend effect. Instruments with obvious trends included SNPP-VIIRS and most of the GOES series through GOES-15 (panchromatic bands).

The independent variable x in SLIMED trends is years after launch. Five forms were studied; any c in the exponent is $-1/\tau$. (1) $y = c_0 + c_1 x$, (2) $y = c_0 e^{c_1 x}$, (3) $y = c_0 + c_2 e^{c_1 x}$, (4) $y = c_0 + c_2 e^{c_1 x} + c_3 x$, and (5) $y = c_0 + c_2 e^{c_1 x} + c_3 e^{c_4 x}$.

For form 5: First, solve form 3 for its τ_3 and then constrain $0 < \tau_1 \leq \tau_3$ and $\tau_4 > \tau_3$. Simply to avoid more complexity, the trend form is constrained to be the same for all bands of an instrument. The quality metric (QM) for trend fits is the normalized decrease of the StDev σ of the calibration ratio weighted by $1/U^2$

$$Q_j = \frac{\sigma(R_j)}{\langle R_j \rangle} - \frac{\sigma(R_j/y_j)}{\langle R_j/y_j \rangle}, \tag{9}$$

where R_j is the set of calibration ratios in band j and y_j are the fit points to those data. QM can be small negative. For an instrument, QM is averaged over all bands. For instruments with significant change, it was found that form 4 is generally the best or close to it. Form 1 is used for instruments with little change. An example of QM for the bands of SNPP-VIIRS for each of the five forms is shown in Fig. 4; for SNPP-VIIRS, form 4 is generally significantly better and never worse than the lower forms, form 5 is fragile (can yield very large τ), and was never a significant improvement over form 4.

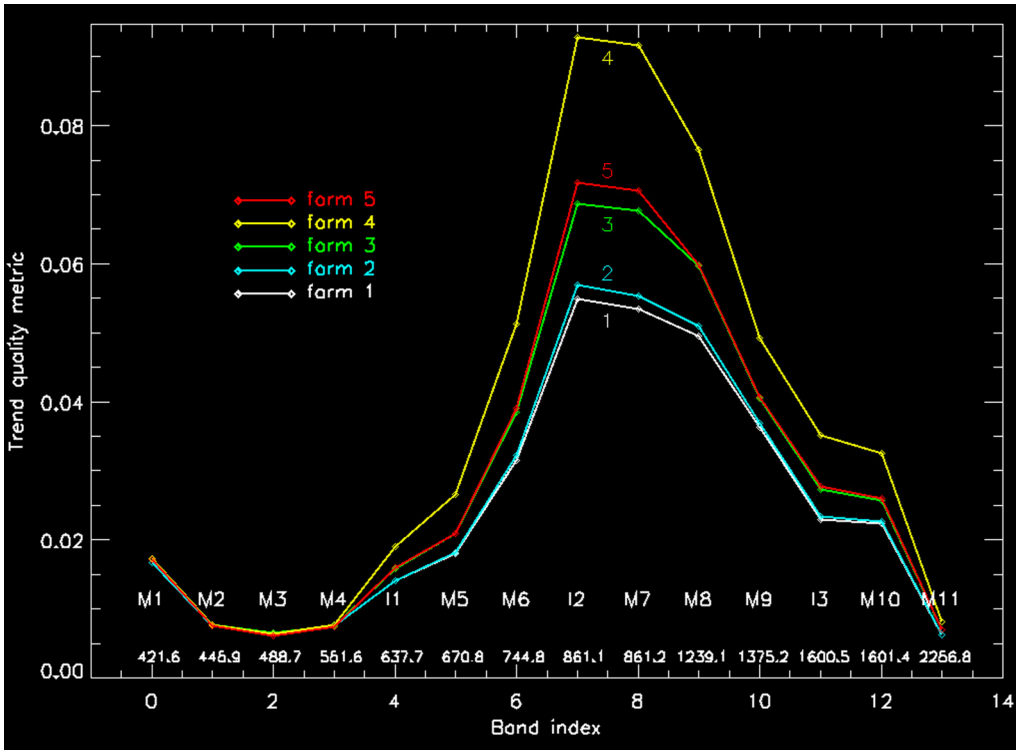

Fig. 4 QM for all five trend forms for all bands of SNPP-VIIRS.

4 Results

A performance metric for MapLib libration models (PML) was defined as the ratio of the StDev of the fit residuals to the StDev of the data; basically, the fraction of the variation that is not captured. The terms can be ranked by a measure of effective magnitude, defined as $|d_j|\sigma_j$, where d_j is the coefficient and σ_j is the StDev of BF j. Libration models were derived using each of the three wave modes, with similar results. The ln λ mode is used for consistency with the SLIMED model fit. From an initial fit with all 108 terms of Eq. (3) and PML $= 0.1075$, the smallest terms were progressively dropped until the PML started to rise significantly; a model with 24 terms was chosen, listed in Table 3, with PML $= 0.1219$.

Decisions on which instruments to fit, hefts to use, BFs to include and values for several convergence parameters are largely a matter of reducing residuals versus increasing complexity. Modestly different choices yield similar models, with the relative empirical gains between instruments being little changed. The SLIMED models are currently based on data from nine LEO instruments and three surface observatories. GEO instruments, apart from ABI16, were found to have more "noisy" calibrations, see Fig. 8. Panchromatic bands, $\frac{\Delta\lambda}{\lambda} \geq 0.2$, were omitted from the fit. For the Base model, only SNPP-VIIRS uses trend-correction before fit. Including an instrument with trend corrections involve iterations to generate a model, calibrate the observations, develop trends, and apply them to observations to be included in fitting the next model.

The spectral irradiance models discussed here are listed in Table 4. The Base model uses MapLib, includes solar variation for all data, uses ln λ as "wave" and includes all the terms listed in Table 5, which lists the resulting coefficients. The Heft terms used for this model are in Table 2. Including MapLib means that the libration terms, lines 22 to 33 in Table 5, need to deal only with MapLib deficiencies. For the Base model, there are 168 bands with initially a total of 89,971 points. After rejection of outliers and within the phase angle limits, 85,924 are used in the final fit; these values are similar for all models incorporating 12 instruments. The "Balan" model includes only instruments for which the wax and wane points roughly balance; ROLO and AeroNet, SeaWiFS, both PLEIADES, and the pair of MODIS instruments that balance each other; a total of 96 bands and 74,730 points are used in the final fit. The last stage was to generate

Table 3 Coefficients of the map-based libration model with 24 terms; coefficients and formal uncertainty multiplied by 1000. Fit based on Eq. (3) and variables scaled as described there. p is signed phase angle in radians, x is Vlon/10 deg, y is Vlat/10 deg, z is Hlat in degrees, w is ln wavelength in μm.

Term	Coef $\times 10^3$	sig $\times 10^3$
x	11.827	0.176
y	−7.031	0.148
z	−0.916	0.080
x^2	3.642	0.211
y^2	−2.254	0.405
yz	0.920	0.101
px	−22.691	0.484
p^2x	1.096	0.445
p^3x	13.967	0.719
p^4x	−3.576	0.189
p^5x	−4.166	0.236
py	−8.709	0.689
p^3y	2.742	1.023
p^5y	−0.826	0.336
pxy	−3.428	0.200
p^2z	−0.536	0.068
px^2	4.410	0.131
p^2x^2	−3.413	0.427
p^4x^2	2.216	0.178
py^2	5.732	0.944
p^2y^2	2.474	0.303
p^3y^2	−6.290	1.383
p^5y^2	1.845	0.454
wpx	−3.418	0.285

a model including the trends derived using the Base model and using the version of the ROLO dataset based on the HSRS solar spectrum (see Appendix A); the result is the V1 model.

The fractional difference between the Base model and all others is shown for zero libration and the GEO phase-angle set in Fig. 5. Models that change the weighting of input data result in brightness differences of roughly 2%; up to 8% for extreme geometries at the longest wavelength. Changes to the fitting parameters yield normalized brightness differences mostly <1%. Statistics on the differences between models, based both on irradiances on the GEO grid and on calibration results, show that changes related to instrument set, heft, or wave mode are on the order of 1% while those related to the other fit options here are on the order of 0.1%.

Quantitative lunar calibration is the ratio of the instrument measured irradiance (adjusted to standard distances) to the model irradiance, often expressed as a percentage difference from one.

Table 4 SLIMED models discussed here, with the variation from the Base model. Items not mentioned are identical to the "base" model. Column 2 is the performance metric in units of 0.01%. Column 3 is the mean absolute difference of the band average calibration from those of the Base model, in %. Column 4 is the mean absolute difference from the Base model using the GEO grid and GSICS bands, in %; the longest wavelengths dominate the change.

Title	PM	del	grid	Description
Base	60.9	0	0	Wave as $w = \ln \lambda$. Heft B; BF as listed in Table 5. Includes MapLib and solar variation
Balan	70.2	1.38	1.05	Includes only data-sets with a similar number of wax and wane observations
w1:lin	65.0	1.39	1.79	Wave as $w = \lambda$
w2:inv	62.1	0.59	0.72	Wave as $w = 1/\lambda$
H1	63.1	1.67	1.30	All heft factors set to 1
Hu	58.6	1.82	2.05	Heft factors set to yield approximately uniform weight for all instruments
−Sv	60.9	0.01	0.01	No solar variation considered
−Map	62.8	0.07	0.54	No use of MapLib
−Lib	70.7	0.11	0.46	Omission of 12 libration BFs
+wavepow	60.2	0.15	0.27	Add 13 BFs with higher wave powers
V1	40.7	0.39	0.23	Correct for trends derived from Base model, ROLOH instead of ROLOG

The final empirical gain for each band is the average of this over date weighted by 1/uncertainty; points with g outside the range for model fit have 1.0 added to their uncertainty, decreasing their weight by a factor of about 400. For instruments used in a fit, this differs negligibly from the final gain computed in the fit process, G_j in Eq. (5). For convenience in displaying calibration results for OLI, the calibration was averaged over the 15 observations obtained within 2 h on each date, covering the 14 identical blocks of detector arrays.

The Base model was used to calibrate all instruments, then look for trends in instruments (except those with a single date) and select a trend form. The results are summarized for all instruments and bands in Table 7, including the mean calibration ratio (col. 4), the StDev over time (col. 5), the magnitude of trends (cols 9:11), and the extent to which the trend model fits the gain history (col. 14).

Calibrating many instruments against one model reveals both similarities and large differences, Figs. 6 and 7. Some of the LEO and surface instruments have offsets fairly consistent over wavelength, Fig. 6: SeaWiFS −4%, ROLO using HSRS −7%, Hyperion +22%. The offset for the two versions of ROLO are similar, but the new version has less scatter. Both PLEIADES, both MODIS, ABI16, AerN, and NIST cluster below 1000 nm near +1%, see also Fig. 14.

5 Discussion

The SLIMED formulation represents the Moon by its disk-equivalent-reflectance and isolates this from the complex spectrum of the Sun and its variability. With a library of many instruments and a model generation system with many parameters, the SLIM system can produce many spectral irradiance models. The Base model presented here represents individual judgment on the weights assigned to instruments and BFs to be included. Application of this irradiance model reveals that over 400 to 870 nm, the group of OLI, both MODIS, both PLEIADES, GOES-16 ABI and two surface observatories calibrated against laboratory standards rather than

Table 5 Coefficients for all BFs of the Base model and the V1 model. The symbols are described in Sec. 1.2, w is natural log of wavelength in μm. In the right six numerical columns all values are multiplied by 1000. The third column is the coefficient; fourth column is the formal uncertainty of the coefficient in the SVD fit. The fifth column is the "importance" of the BF as measured by the absolute value of the coefficient times the StDev of the BF. Columns 6 to 8 are the values for the final model discussed here, V1.

		Base = 22Apr16T1827			V1 = 22May28T1548		
I	Symbol	value $\times 10^3$	uncert $\times 10^3$	val $\times$ StD $\times 10^3$	value $\times 10^3$	uncert $\times 10^3$	val $\times$ StD $\times 10^3$
0	1	165.933	2.82187	0.000	160.471	2.86976	0.000
1	w	2.361	2.48288	1.026	21.261	2.54409	9.210
2	w^2	−95.281	3.02417	24.203	−95.600	3.07038	23.997
3	g	−1243.839	1.73058	515.531	−1234.935	1.71108	509.973
4	g^2	151.422	3.26420	88.952	139.370	3.37072	81.269
5	g^3	−154.345	4.20604	122.599	−149.600	4.33973	117.620
6	gw	279.268	1.85148	98.557	250.609	1.78433	87.556
7	gw^2	−29.627	2.94323	6.525	−24.373	2.79679	5.260
8	g^2w	−89.973	9.14530	35.644	−78.435	9.39848	30.637
9	q	4.816	10.87541	14.459	5.146	11.15408	15.449
10	q^2	0.306	9.70104	9.634	0.301	10.10182	9.466
11	qw	−8.662	1.77229	19.535	−12.735	1.66997	28.769
12	qw^2	0.738	9.98481	1.141	0.427	10.37717	0.660
13	q^2w	0.309	23.20380	6.227	0.538	22.67480	10.835
14	h	49.458	28.01185	37.971	48.971	28.87266	37.469
15	h^3	11.279	3.13963	11.016	12.558	4.20469	12.150
16	h^5	−4.722	0.40499	7.858	−5.171	0.37757	8.480
17	hw	4.606	1.16928	1.849	3.820	0.97497	1.522
18	hw^2	−8.007	0.97728	2.273	−7.464	0.99700	2.088
19	h^3w	−0.824	0.67489	0.418	0.334	0.64279	0.167
20	z	−0.024	0.89116	0.026	0.204	0.79356	0.218
21	zw	−0.307	0.82406	0.181	0.043	0.77641	0.025
22	x	−0.808	0.54739	3.562	−0.750	0.54813	3.300
23	y	−0.340	0.47219	1.639	−0.383	0.48505	1.847
24	x^2	−0.002	0.12142	0.038	−0.004	0.12132	0.061
25	y^2	−0.009	0.12752	0.158	0.006	0.13697	0.109
26	xw	0.053	0.24935	0.126	0.020	0.25262	0.046
27	yw	0.253	0.22680	0.674	0.143	0.22894	0.380
28	(hx)	−0.429	0.16818	1.609	−0.450	0.17355	1.683
29	(hy)	0.032	0.11829	0.123	0.063	0.12172	0.242
30	$(hx)^2$	0.008	0.04717	0.177	0.006	0.05016	0.135
31	$(hy)^2$	0.004	0.03287	0.080	−0.010	0.03345	0.222
32	$(hx)w$	−0.115	0.01492	0.227	−0.062	0.01519	0.121
33	$(hy)w$	−0.158	0.03187	0.322	−0.044	0.03224	0.088

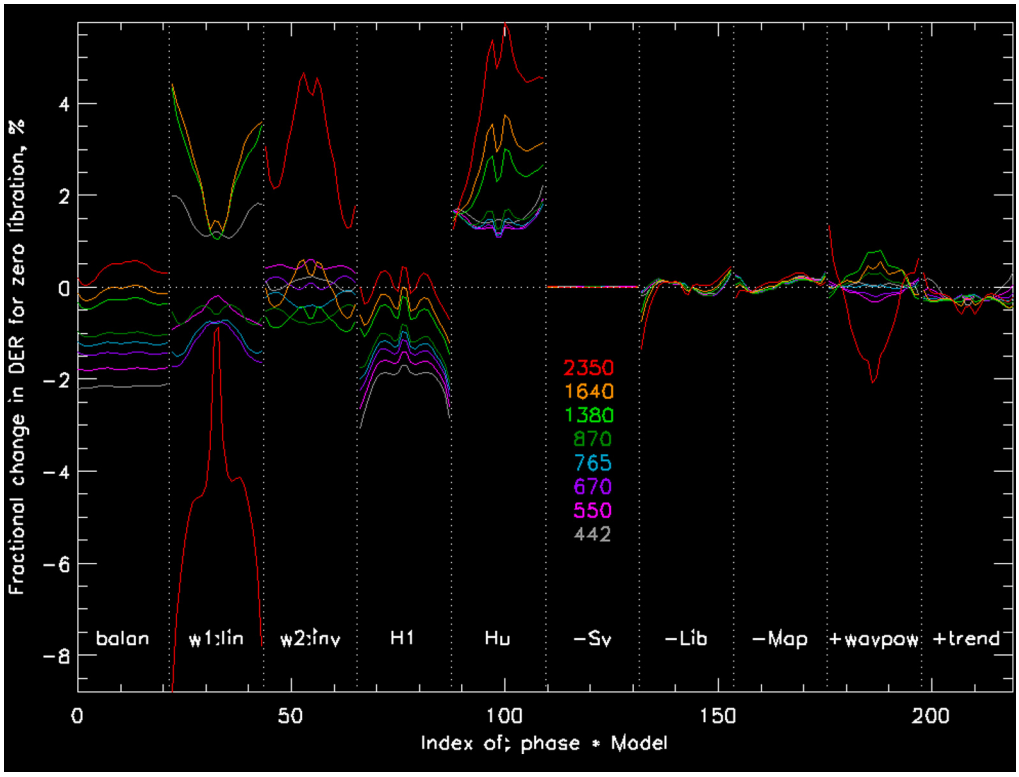

Fig. 5 Average change in DER from the Base model at zero libration over the GEO grid. In each panel phase angle increases from left to right. Models left of the legend involve different instrument sets, wave-mode or heft; those at or to the right involve change of fit parameters. "+trend" is the V1 model.

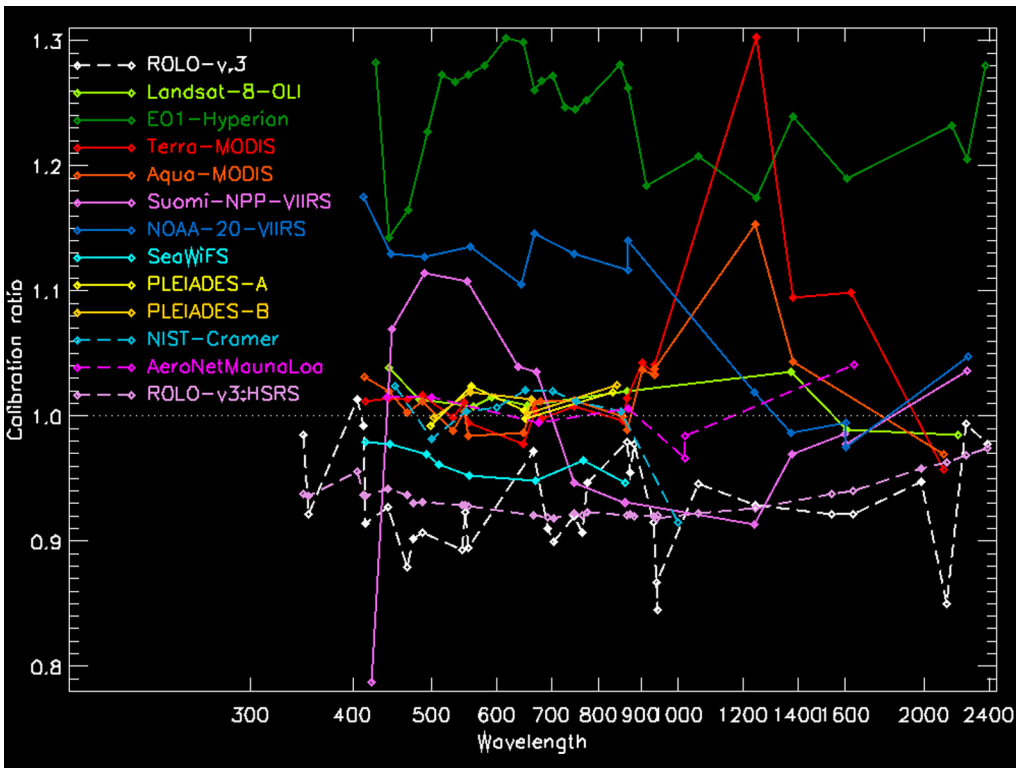

Fig. 6 Calibration of LEO (lines) and surface instruments (dashed) with the Base model showing the average over time for each band, with two versions of the ROLO dataset.

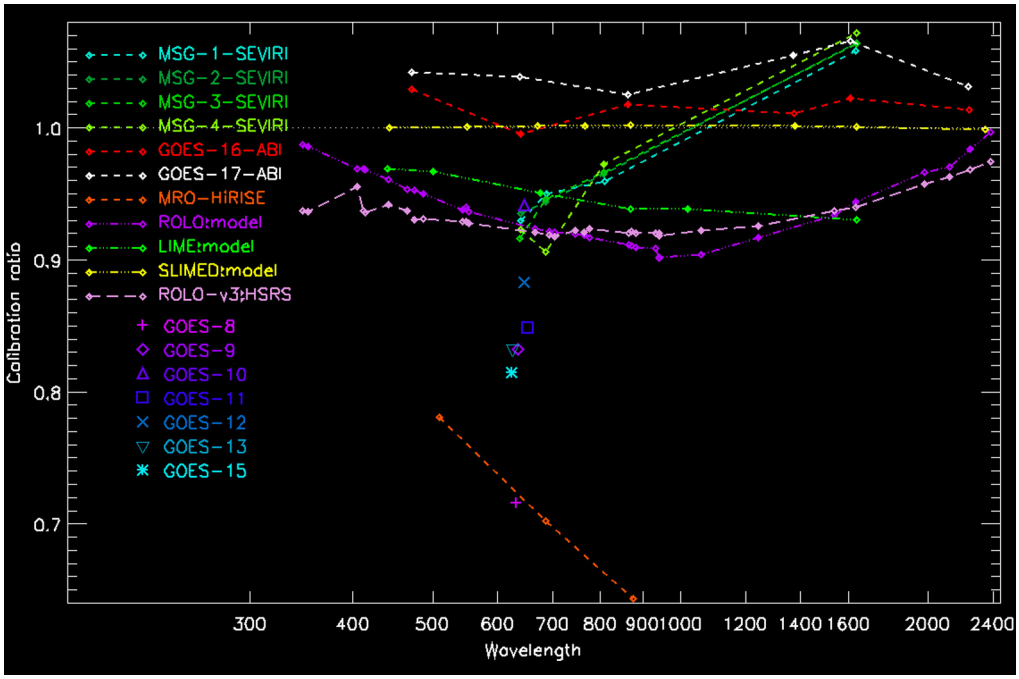

Fig. 7 Calibration of GEO, farther away, and some models (dash dots) with the SLIMED Base model. GOES pan bands are solitary diamonds. The ROLO entry is ROLOH; the version 3 dataset using the HSRS. Model entries (dash-dots) are evaluated on the GEO geometry grid.

stars, NIST and AeroNet, agree within a few percent, averaging about 1% above the model; Fig. 14. Considering the gain-adjustment used in SLIMED models, it is plausible that the real Moon lies in this cluster and that the Base model is about 1% low in this wavelength region. Although the LIME model is traceable to a cryogenic radiometer and "has an expanded ($k = 2$) absolute radiometric uncertainty of ~2%",[12] it is 4 to 7% below this group. The ROLO/GIRO model is 5% to 10% lower than this group, Fig. 7. These relative values are consistent across SLIMED models resulting from modest changes in model inputs.

The scatter (standard deviation) of calibration over time for each band is a measure of the consistency of the instrument's lunar observations, shown in Fig. 8. All GEO instruments except ABI16 show more scatter than LEO instruments. The GOES 8 to 15 series, after correction for trends, have a few percent scatter but no clear dependence on phase angle. The calibration ratio including trend corrections (forms listed in Table 7) for the bands of each fit instruments and GOES-ABI's were normalized to average one, then the average over band for each instrument was plotted versus time, Fig. 9. While there are some seasonal oscillations near the 1% level, there is no apparent phase coherence across instruments, which if present would suggest a problem with the model. However, the b_{jk} in Eq. (4) are relatively low at both ends of the spectral range overall phase angles, suggesting that the lunar reference spectrum, based on disturbed lunar soil samples, is too bright at both ends.

Both PLEIADES made frequent observations during one lunation, see Fig. 3. In particular, PleB made 227 observations in 15.8 days centered on full Moon, covering −101.5 deg to +101.6 deg phase. The calibration results (including trend correction, which is small) for this phase-angle sweep, Fig. 10, provide a test of the model. For 10 deg $< g <$ 60 deg deviations are <0.5%. However, under $g = 5$ deg the calibration drops sharply indicating a model of the opposition effect more sophisticated than the simple polynomial in $1/g$ used here is needed for calibration at such small phase angles.

5.1 *Examples of Trends*

Table 7 has the calibration trend results for all bands of instruments with more than one date. The trend form used is the simplest that captures the instrument behavior. These continuous

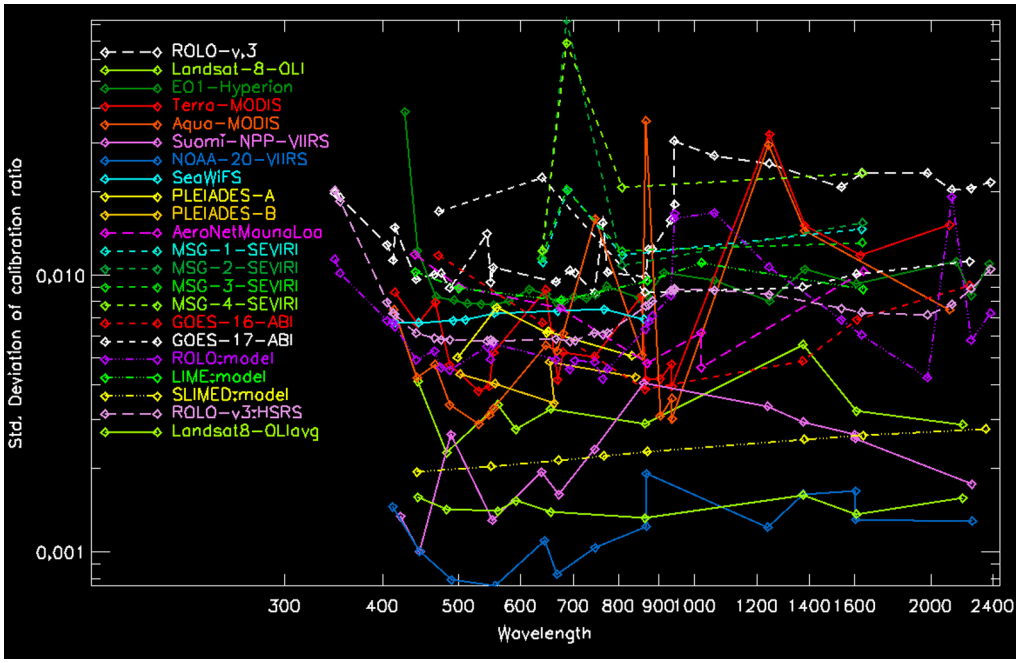

Fig. 8 Standard deviation of the calibration ratio for most instruments with trend correction using the Base model. GEO instruments are shown dashed; single-band GOES are single diamonds near 650 nm. SEVIRI are largely above 10%, suggesting problems in processing images to irradiance; a couple MODIS bands are also high, as are ROLO version 3 SWIR bands. There are two curves for OLI, the lower one is for data averaged over the 15 observations on one date.

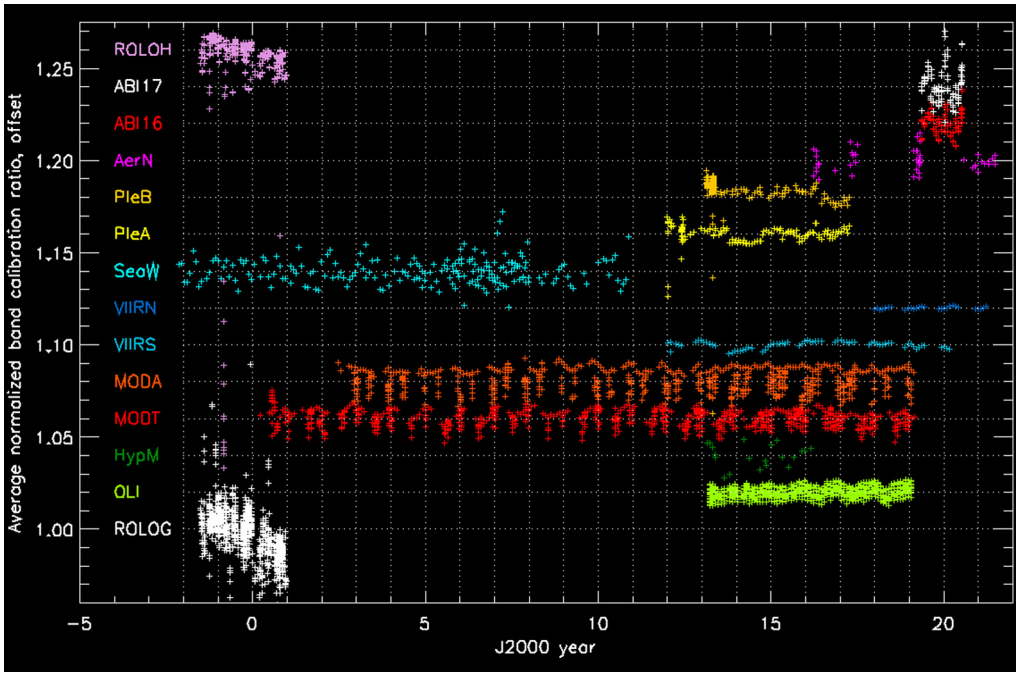

Fig. 9 Instrument calibration versus date using the trend forms listed in Table 7. Average calibration ratio over instrument bands for each date, then normalize each instrument to a grand average of one. Each symbol is one date. Instruments are offset by 2%. Dotted lines at the beginning of each year.

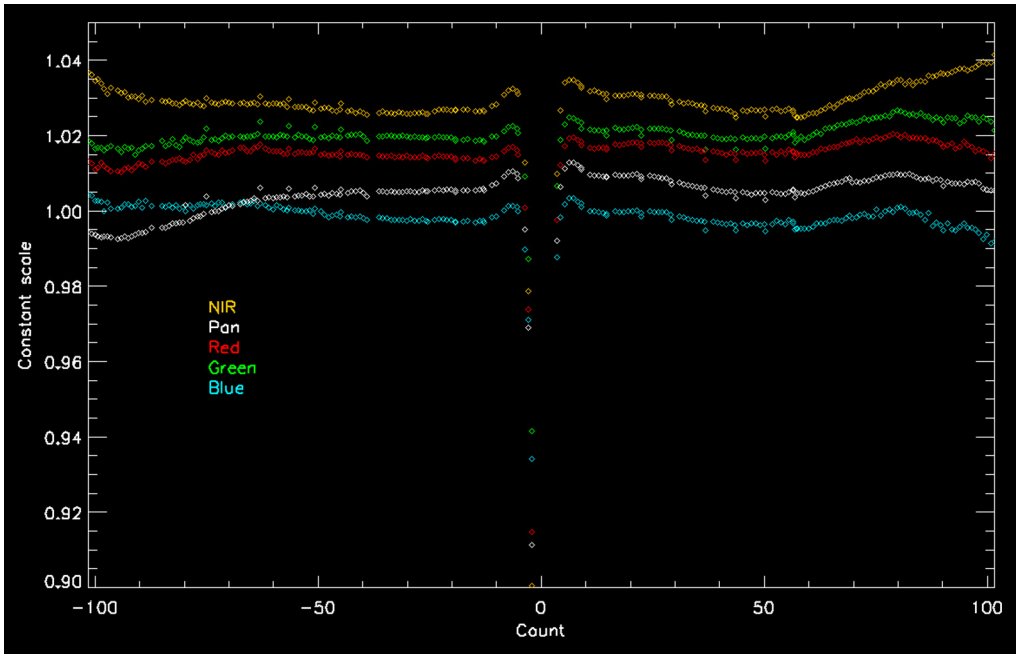

Fig. 10 Calibration using the V1 model of PleB during its dense coverage of one lunation. The small correlated jumps in both waxing and waning phase are when observations were spaced by >0.3 deg phase (36 min of time) and may be related to location of the spacecraft along its 98.7-min orbit.

forms do not deal with the many styles of events that can cause offsets in response or their rates of change.

OLI was calibrated and trended using both the Base and the V1 model, results are nearly identical. Only the coastal aerosol band (443 nm) has discernible early decrease, Fig. 11.

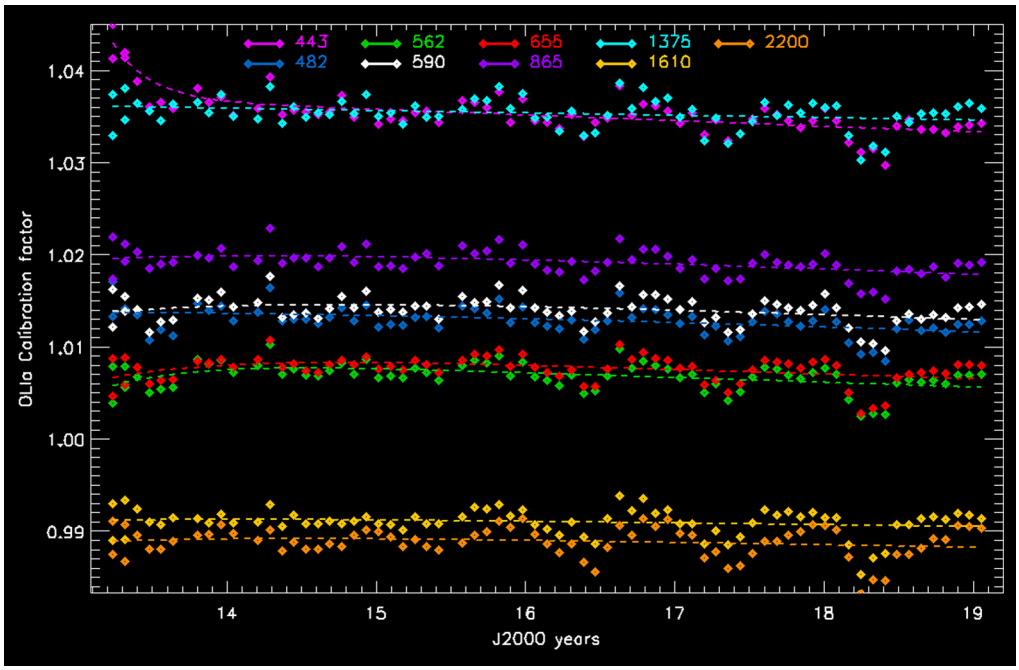

Fig. 11 Calibration of OLI using the V1 model. The first two lunations (during commissioning) had two raster sets. Dashed lines are the form 4 trend fit.

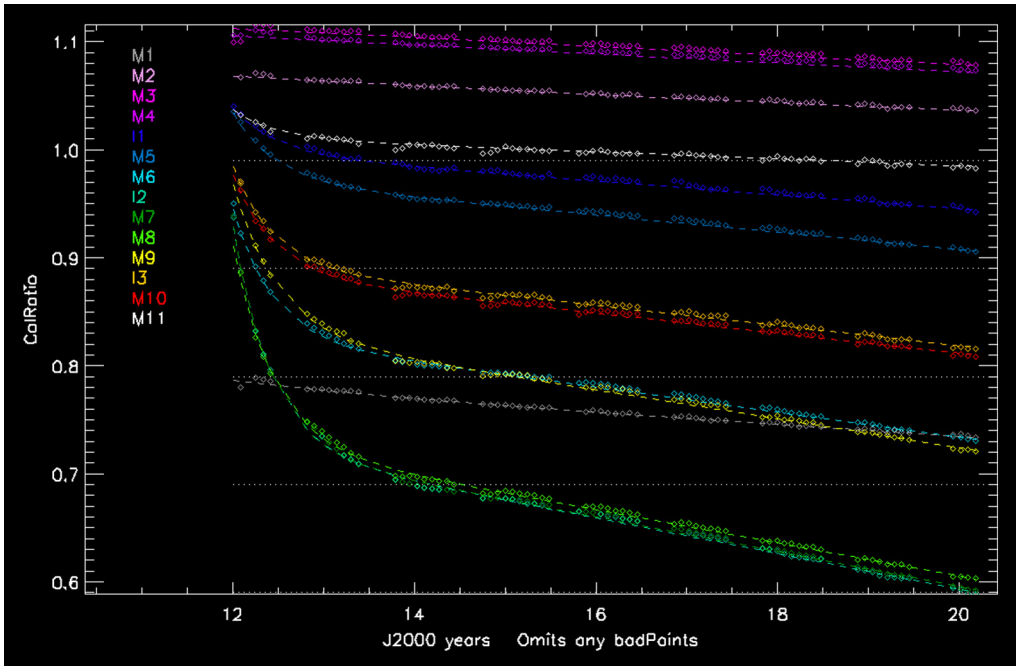

Fig. 12 SNPP-VIIRS calibration using a form = 4 trend fit. Diamonds are the calibration ratio, dashed lines are the trend form four fit. Dotted line are constant-value guides. Several bands show a small rise early in each of the years 2014 to 2016.

The pan, green, and red bands show a small initial rise of about 0.02%, probably due to inconsistencies in procedure or processing during commissioning. After the first two or three years, there is a clear annual variation in all bands of about 0.4%. For OLI, except for Coastal Aerosol (Aer), QM for all forms and bands is small, <0.02%; Aer reaches 0.1% for forms 4 and 5, which capture the early drop in response. However, the low QM does not justify any form above 3 for the other bands. All OLI bands drop about $\frac{1}{2}$% over 6 years, fairly small compared to the scatter. The OLI full-resolution calibration data would support a study of the gain history of all 126 detector arrays in OLI.

Calibration for SNPP-VIIRS using the Base model shows an initial asymptotic drop and a continuing linear trend, well fit by form 4, Fig. 12. The StDev of residuals from the trend-fit is 0.30% and there is an indication of an about 0.02% annual or semiannual oscillation on top of the much larger trend. NOAA20-VIIRS (VIIRN) shows little trend, form 1 has a linear coefficient of about 0.1%/year or less.

As ROLO data are calibrated against stars every night, trends were not expected. However, the band near 2250 nm has a linear trend of +3.2% per year and the other bands average +1%. One possibility is a gradual increase in scattering in the telescopes that led to a drift in the calibration of point sources relative to the lunar integration.

Among GEO instruments, lunar calibration for all except GOES-16 ABI is noisier than operational LEO instruments, see Fig. 8. The early GOES series generally have strong trends; Table 7. For both ABI's, trends are small for all bands, but there is about 1% to 2% scatter at each lunation. Also, both ABI's show an increase in calibration ratio with an absolute phase angle of about 2%; the reason for this is unknown.

6 Conclusions

A methodology for incorporating multiple sources of information on lunar spectral irradiance has been developed and applied to generate an improved lunar model useful for instrument radiometric calibration. This addresses the major known issues with the ROLO model, listed in the introduction. SLIMED models are continuous in wavelength and all geometry parameters,

as must be the actual Moon, and the full prescription is given here. The "V1" model, resulting from using the trends derived with the Base model, is thought to be closest to the actual Moon; V1 supports trending at the 0.1% level. SLIMED models are based on 12 times the number of instruments and three times the amount of data as the ROLO/GIRO model, have 1/10 the number of coefficients and 1/2 the magnitude residuals. Applying the SLIMED Base model to 25 instruments and two other models reveals some encouraging consistencies and some large differences.

It seems implausible that the geophysical products of these instruments, used by the world's scientific community, can have differences as large as indicated by lunar calibration. Thus, something is amiss in the lunar calibration of at least some of the instruments, either in the observations or the processing to irradiance. The realities of comparisons based on a single model of the Moon need to be examined and resolved before the full potential of lunar calibration can be realized. Observing the Moon with the same optical configuration as science targets should help, especially for absolute calibration. There is no barrier to a lunar model, and even lunar calibration, eventually achieving accuracy at the 0.1% level.

SLIMED was developed in IDL, which is a proprietary language but is common within NASA. When implemented in an open language, the SLIMED concept can be used to generate an up-gradable reference model for the lunar calibration community. The methodology could weigh heavily accurate, traceable, above-the-atmosphere measurements of lunar irradiance; such measurements do not yet exist. In the future, the lunar calibration community could be involved in setting the weights assigned to the source data and in other decisions, leading to a "consensus" model.

7 Appendix A: Instrument Data

MODIS, Terra, and Aqua. On MODIS-Aqua (MODA), the 1630-nm band is noisy and was omitted. Description of Lunar observations and comparison with PLEIADES is in Refs. 41–43.

Sea-viewing Wide Field-of-view Sensor (SeaWiFS) was the first operational instrument to do regular lunar calibrations. SeaWiFS did reverse-pitch attitude maneuvers to view the Moon directly on most months for 13 years, concentrated near $p = \pm 7$ deg; there are also about 60 early observations at large phase angles. Its 1.16-mrad resolution yields about 6 pixels across the Moon. Lunar calibration was used extensively in developing the final response history for SeaWiFS. All the lunar observations described in Ref. 44 are included here.

Operational Land Imager, Landsat 8 (OLI) is a push-broom imager with 14 blocks of detectors cross-track. OLI did reverse-pitch attitude maneuvers to view the Moon directly,[45] scanning in a raster pattern so the Moon passed through the center of 7 or 8 of its 14 focal-plane-modules. OLI data are available for 72 lunations at similar phase angle; each raster pair was acquired on successive orbits in 113 min, within which the optical libration variation is largely due to N–S spacecraft motion. For convenience in displaying calibration results, these were averaged over each raster-pair for each band to form a virtual instrument assigned the acronym OLIa; the full-resolution data are always used in the model generation.

Visible Infrared Imaging Radiometer Suite; Suomi NPP (VIIRS). SNPP VIIRS showed a significant drop in response over the first 400 days on orbit.[46] Lunar views are obtained through a spaceport during spacecraft day, using scan-mirror angles different from ground scenes.[46] Lunar observations are described by Refs. 47 and 48. The team analyzed these data using the ROLO model.[48–50] Suomi-VIIRS has a known problem of degradation of scan-mirror coatings, which has been monitored by its solar diffuser. Eplee et al.[50] analyze this in detail using both the on-board solar diffuser and lunar calibration with the ROLO model; their Fig. 4 shows most months from January 2012 to June 2019. They fit $A_0 - A_1(1 - e^{-\tau(t_s - t_0)})$ with $\tau = 1/2000$ days with roughly 0.5% annual residual. Here, trends are based only on lunar calibration using SLIMED models. The scan mirror degradation has a spectral component, which would result in small changes to the equivalent wavelength of some bands; this is not addressed in the SLIM system.

Visible infrared imaging radiometer suite; NOAA-20 (VIRRN). Similar to VIIRS, but this second instrument avoided the mirror-coating issues; bands have little trend.

The PLEIADES spacecraft are agile and point directly at the Moon from many places along their orbits. PLEIADES 1A and 1B made observations over a wide range of phase angles, including dense sets in a single lunation;[51] 1B made additional dense lunation sweeps but these were not provided. The team provided trend information as calibration factors for each band every 3 months. These factors are close to linear with time and were treated as piece-wise-linear in application to the measured irradiances.

Hyperion is a spectrometer on the EO-1 spacecraft with VIS and near-IR focal planes, which have overlapping wavelengths.[52] Each section has bands of negligible response at its low and high wavelength ends. Omitting these bands and the less-responsive bands in the overlap region leaves 204 bands of about 10.5-nm resolution covering 427 to 2400 nm with crossover near 916 nm. The level 0 ancillary data and level 1 images were processed by the author to lunar irradiance values, independent of the lunar calibration of Ref. 53 but with similar results. Hyperion did attitude maneuvers to scan across the Moon; the cross-track width was barely larger than the Moon and incomplete coverage scans are not included.

The first eight Geostationary Operational Environmental Satellites, GOES-8 to -15, had a single broad band in the solar-reflectance regions, 0.5 : 0.8 μm; no data was available for GOES-14.

GOES-16 and 17 carry the advanced baseline imager (ABI), which has six solar-reflective bands.

The Spinning Enhanced Visible and InfraRed Imager (SEVIRI) instruments are on four Meteosat second generation (MSG) geostationary spacecraft; descriptions of lunar observations are in Refs. 4 and 54. The instruments have four solar-reflective bands, one of which is very wide, 0.4 : 1.1 μm. Various bands were listed as valid as a function of date and some of these were calibration outliers. About 28% of the total points were rejected for each instrument.

The ROLO ran during the bright half of each month on clear nights for nearly 7 years. The version 3 dataset, source of the 311g model,[3] was used with the acronym ROLOG. Formal uncertainties were provided for each point; these do not include the much larger absolute scale uncertainty of about 5%;[55] thus the provided uncertainties were scaled to average 5%. A second version of the irradiances, developed using the recent HSRS[34] was provided by Tom Stone and is assigned the acronym ROLOH.

National Institute of Standards and Technology (NIST). Surface observations from an observatory in Arizona. Data are extracted from Table 1 of Ref. 39, which is for a single time and includes uncertainties (data were duplicated to avoid processing complications). Initial analysis suggested that the longest wavelength irradiance is errant, and its published uncertainty was arbitrarily tripled.

AeroNet lunar observations using CIMEL photometers on Mauna Loa at 3402-m elevation used a NIST-traceable calibration, with nightly Langley plots to determine atmospheric attenuation.

High Resolution Imaging Science Experiment (HiRISE). An instrument of extraordinary angular resolution and calibration challenges made a few observations of the Moon from Mars. The Moon is resolved with about 8 pixels across the lunar diameter (similar to SeaWiFS).

8 Appendix B: Error Estimates

Estimates of possible errors are listed in Table 6. There are uncertainty values for typical current practice and after potential improvements over the next decade or so. Some can be calculated based on an image time error or spacecraft location error, some are rough estimates, and some are known to be so small that at worst they are negligible.

Table 6 Estimates of sources of error in lunar calibration. "Value" is the current or typical value; "est." = estimated. Last two columns are effect on an irradiance calibration in ppt. Typical: Magnitude if ignored or an estimate at current practice. Best: Rough forecast considering best practice perhaps a decade in the future.

		In ppt	
Item	Value	Typical	Best
Model: absolute	est. 3%	30	5
Model: relative	est. 0.5%	5	1
Maneuver from Nadir: hardware	est. 2%[a]	20	1
Image artifacts: ghosts, flare	est. 1%[a]	10	1
Oversampling factor (now commonly poorly known)	1%[a]	10	0.1
Pixel scale change cross-track, e.g., for OLI	0.5%	5.8	0.01
Scan uniformity[b]: $\epsilon \cdot \nabla I$	est. 1/200[a]	5[c]	0.5
Frame image distortion, residual: $\sim \propto \theta^3$, use 2 deg	4×10^{-5}	0.04	0.04
Polarization: lunar times instrument[a]	Moon max. is 9%[d]	25	1
Image processing to irradiance, corrected for above	0.1% to 3%	1 to 30	0.1
Solar variability, most in UV	$\sim$1 W/m^2	0.7	0.1
Image time: distance and libration: 1 s $\sim$7.6 km	5.2×10^{-4}	0.4	0.04
$1/r^2$ approximation, out to GEO	5×10^{-4}	0.5	0.05
Moon not a sphere: $\Delta h/R \sim 1/1737$ local[e]	2×10^{-4}[f]	2	<1
Below are negligible at worst	—	—	Worst
Spacecraft ephemeris: one axis	est. 0.1 km	2.6×10^{-4}	$\ll$1
Lunar surface global reflectance change[g]	1×10^{-8}/year	2×10^{-4}	$\ll$1
Relativity: time[h]	$d/c \sim 1.3$ s	1.4×10^{-8}	$\ll$1
Relativity: Aberration	$v/c \sim 2 \times 10^{-5}$ radian	3×10^{-6}	$\ll$1
Lunar ephemeris	10 cm	2.6×10^{-8}	$\ll$1

[a]May vary widely between instruments.
[b]Fractional rate change while crossing the Moon, e.g., change in mean scan rate over first 1/2 Moon to second 1/2.
[c]Depends upon scan direction. Typical proportional radiance difference between two halves of a lunar image may be 10%.
[d]Varies with phase angle and wavelength.
[e]Nonlinearity in $1/\cos\theta$ over 7 deg $[1.2 \times 10^{-3}]$ for LEO; times the fractional circumference. Arbitrarily set at $\frac{1}{4}$ topography/radius. It is covered by libration terms.
[f]Accounted for in libration terms in model.
[g]Barring major human activity on the Moon.
[h]Maximum effect on d is 0.11 km.

9 Appendix C: Supporting Figures

The gain adjustment factors G_j converge asymptotically with each iteration of Eq. 5; the change in G_j typically decreases with each iteration, an example is shown in Fig. 13. By iteration 19, most bands are changing less than 0.01%. The empirical gain, which for instruments fit in the model is almost the same as the final G_j, shown in Fig. 6 is displayed in more detail in Fig. 14. The trends derived with the Base model for all instruments are listed in Table 7. The calendar dates for each instrument are listed in Table 8.

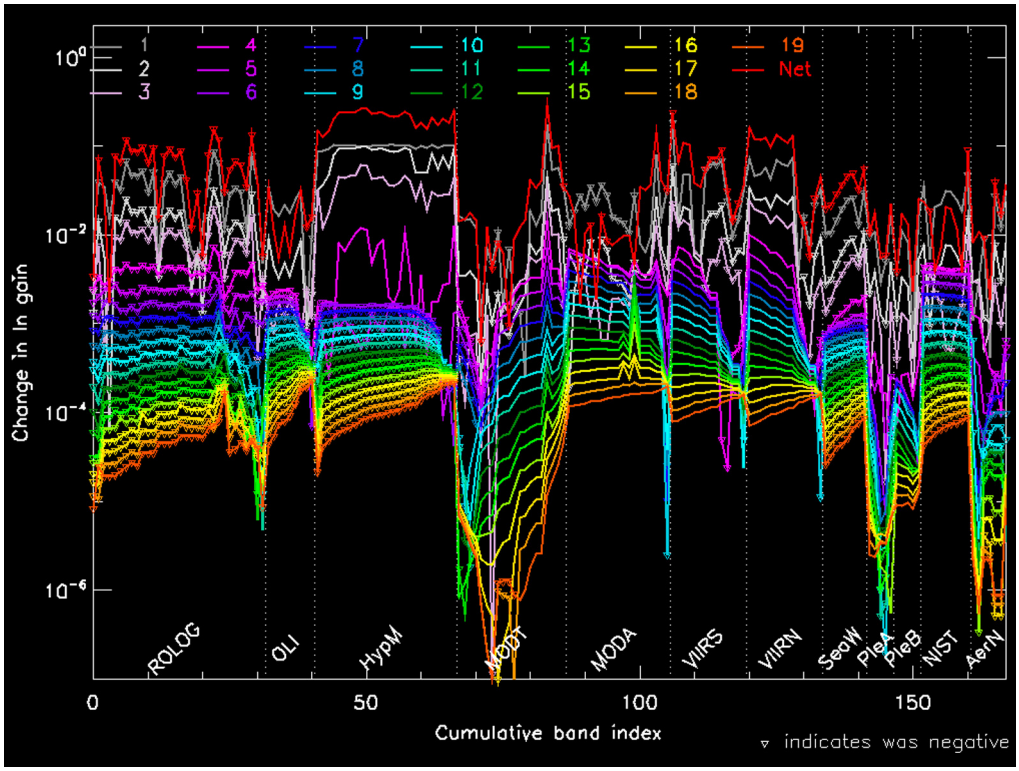

Fig. 13 Convergence of the empirical gain factor for all bands used in the Base model fit. The change in the natural logarithm of the gain factor between successive iteration is shown. The iteration index is indicated in the color legend. Low value in early iterations usually indicate a change of sign. Small triangles indicate the value was negative.

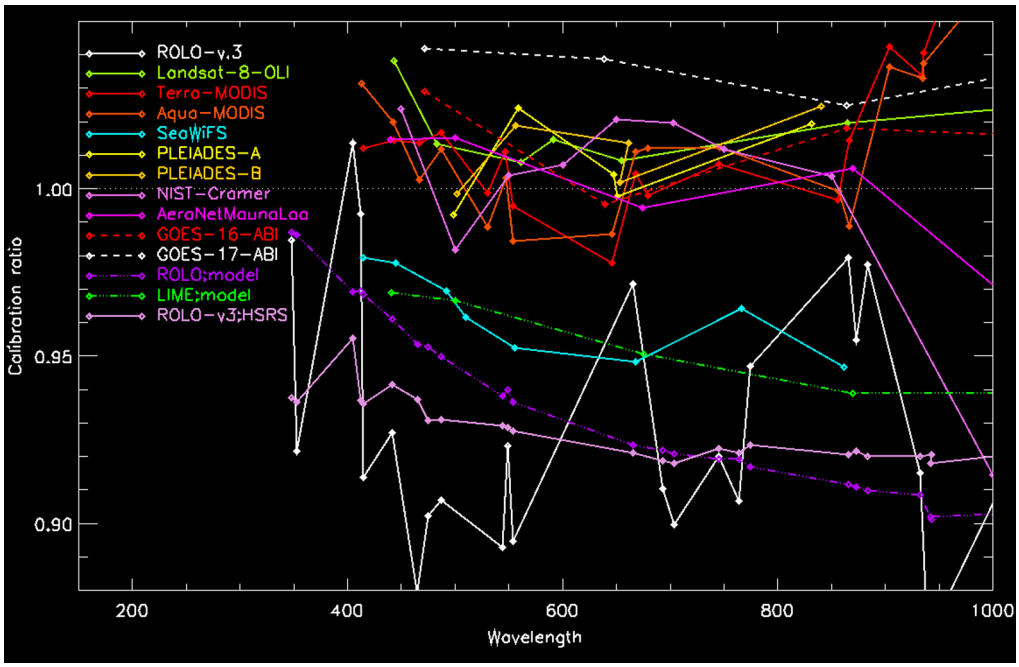

Fig. 14 Calibration of some LEO and surface instruments, both ABI's, two versions of the ROLO dataset, and two models. This enlarges the "cluster" of Fig. 6 omitting the instruments that deviate considerably from 1.

Table 7 Calibration and trends. The instrument title lines contain the acronym followed by the trend form used and the number of dates. All other lines are: Col. (1) is band index within instrument in SLIM; (2) band name; (3) nominal wavelength in nm; (4) mean calibration ratio as % above 1; (5) standard deviation of calibration over time $\times 10^4$; (6) range of calibration, minimum − mean, $\times 10^3$; (7) range of calibration, maximum − mean, $\times 10^3$; (8) fit coefficient c_0; (9) For form 1, fit coefficient c_1, for form 2:5, τ in years; (10 and 11) fit coefficient c_2 and c_3; (12) normalized (σ/mean) weighted standard deviation of the calibration $\times 10^3$; (13) similar to col. 12 but with the trend removed, weighted mean absolute residual from the fit, $\times 10^3$; (14) improvement (decrease) in the normalised standard deviation by applying the trend, $\times 10^5$.

1	2	3	4	5	6	7	8	9	10	11	12	13	14
			Calibration				Trend coefficient				Normalized SD		
Band index	Band name	Wave nm.	Mean	SD	Δ min	Δ max	c_0	$c_1 \vee \tau_1$	c_2	c_3	Cal	−Trend	Imp
—	**ROLOG**	1	1249	—	—	—	—	—	—	—	—	—	—
0	16	345	−1.5	197	−658	230	0.97622	0.00444	:	:	42.7	42.4	26
1	17	355	−7.9	189	−729	221	0.91826	0.00332	:	:	31.8	31.6	21
2	18	405	1.4	128	−82	196	1.00737	0.00602	:	:	16.1	15.5	57
3	2	412	−0.8	112	−62	192	0.99614	0.00144	:	:	11.2	11.1	4
4	19	415	−8.6	148	−540	164	0.91213	0.00376	:	:	18.6	18.3	29
5	4	443	−7.3	96	−52	159	0.92333	0.00329	:	:	19.2	19.0	19
6	20	465	−12.1	99	−65	130	0.87721	0.00307	:	:	18.2	18.0	25
7	21	475	−9.8	101	−70	119	0.89693	0.00496	:	:	23.5	23.1	45
8	6	488	−9.3	89	−55	111	0.90064	0.00470	:	:	20.1	19.7	34
9	22	545	−10.7	140	−292	93	0.89361	0.00393	:	:	13.5	13.0	50
10	8	551	−7.7	93	−74	87	0.92055	0.00452	:	:	9.8	8.9	90
11	23	555	−10.5	106	−80	93	0.89743	0.00328	:	:	11.0	10.6	40
12	10	667	−2.9	94	−74	73	0.97675	0.00216	:	:	9.0	8.8	20
13	24	695	−9.0	103	−89	51	0.91296	0.00359	:	:	11.1	10.7	44
14	25	705	−10.0	101	−90	52	0.90649	0.00132	:	:	12.3	12.1	12
15	12	748	−8.0	85	−63	53	0.92803	−0.00016	:	:	8.4	8.4	0
16	26	765	−9.3	154	−87	60	0.90926	0.00208	:	:	17.9	17.8	19
17	27	775	−5.3	102	−93	49	0.95324	0.00179	:	:	10.5	10.3	15
18	14	869	−2.1	98	−65	58	0.99406	−0.00172	:	:	9.0	8.9	12
19	28	875	−4.5	123	−92	45	0.96565	0.00149	:	:	12.3	12.2	5
20	29	885	−2.3	123	−96	53	0.98851	0.00153	:	:	11.9	11.8	7
21	30	935	−8.5	157	−86	67	0.92138	0.00071	:	:	17.8	17.8	2
22	31	944	−15.5	179	−80	86	0.85726	−0.00026	:	:	23.3	23.3	−1
23	52	945	−13.3	303	−157	151	0.87290	0.00222	:	:	48.6	48.5	6
24	54	1060	−5.4	269	−181	101	0.95192	0.00279	:	:	31.8	31.7	13
25	57	1250	−7.2	251	−157	81	0.93715	0.00032	:	:	41.2	41.2	1
26	58	1550	−7.9	207	−875	81	0.94109	−0.00211	:	:	27.1	27.1	1

Table 7 (*Continued*).

1	2	3	4	5	6	7	8	9	10	11	12	13	14
			Calibration				Trend coefficient				Normalized SD		
Band index	Band name	Wave nm.	Mean	SD	Δ min	Δ max	c_0	$c_1 \vee \tau_1$	c_2	c_3	Cal	−Trend	Imp
27	60	1640	−7.8	232	−573	65	0.94939	−0.00331	:	:	30.2	30.2	2
28	62	1990	−5.2	232	−826	80	0.97785	−0.00367	:	:	31.3	31.3	0
29	64	2140	−15.0	202	−452	101	0.84363	0.00724	:	:	22.1	22.5	−41
30	66	2260	−0.6	204	−96	157	0.97695	0.01620	:	:	28.3	25.3	298
31	68	2390	−2.3	215	−347	67	0.98723	0.00144	:	:	22.8	22.8	3
—	**NIST**	0	2	—	—	—	—	—	—	—	—	—	—
0	450	450	2.4	0	0	0	:	:	:	:	:	:	:
1	500	500	−1.8	0	0	0	:	:	:	:	:	:	:
2	550	550	0.4	0	0	0	:	:	:	:	:	:	:
3	600	600	0.7	0	0	0	:	:	:	:	:	:	:
4	650	650	2.1	0	0	0	:	:	:	:	:	:	:
5	703	703	2.0	0	0	0	:	:	:	:	:	:	:
6	750	750	1.2	0	0	0	:	:	:	:	:	:	:
7	850	850	0.4	0	0	0	:	:	:	:	:	:	:
8	1000	1000	−8.5	0	0	0	:	:	:	:	:	:	:
—	**ROLOH**	1	1249	—	—	—	—	—	—	—	—	—	—
0	16	345	−6.3	201	−82	32	0.92782	0.00322	:	:	29.8	29.7	7
1	17	355	−6.4	184	−84	29	0.92654	0.00322	:	:	28.7	28.6	7
2	18	405	−4.5	79	−102	11	0.94518	0.00340	:	:	25.0	25.0	8
3	2	412	−6.3	72	−101	10	0.92698	0.00331	:	:	25.1	25.0	8
4	19	415	−6.4	71	−101	10	0.92577	0.00333	:	:	25.2	25.1	8
5	4	443	−5.9	61	−104	9	0.93162	0.00334	:	:	25.7	25.6	7
6	20	465	−6.3	59	−104	9	0.92701	0.00334	:	:	26.3	26.2	7
7	21	475	−6.9	58	−103	9	0.92077	0.00332	:	:	26.5	26.4	7
8	6	488	−6.9	58	−103	10	0.92112	0.00331	:	:	26.8	26.7	7
9	22	545	−7.1	57	−102	11	0.91917	0.00334	:	:	27.9	27.8	6
10	8	551	−7.1	58	−101	12	0.91891	0.00331	:	:	28.0	28.0	6
11	23	555	−7.2	57	−101	11	0.91786	0.00334	:	:	28.1	28.0	6
12	10	667	−7.9	58	−95	11	0.91129	0.00331	:	:	29.8	29.8	5
13	24	695	−8.1	57	−94	10	0.90892	0.00334	:	:	30.2	30.1	5
14	25	705	−8.2	57	−93	10	0.90808	0.00334	:	:	30.3	30.3	5
15	12	748	−7.8	61	−92	10	0.91268	0.00336	:	:	30.9	30.9	4
16	26	765	−7.9	60	−91	9	0.91111	0.00339	:	:	31.1	31.1	4

Table 7 (*Continued*).

1	2	3	4	5	6	7	8	9	10	11	12	13	14
			Calibration				Trend coefficient				Normalized SD		
Band index	Band name	Wave nm.	Mean	SD	Δ min	Δ max	c_0	$c_1 \vee \tau_1$	c_2	c_3	Cal	−Trend	Imp
17	27	775	−7.7	61	−90	9	0.91352	0.00340	:	:	31.3	31.2	4
18	14	869	−8.0	76	−84	15	0.91055	0.00341	:	:	32.5	32.4	4
19	28	875	−7.8	77	−83	15	0.91170	0.00344	:	:	32.6	32.5	4
20	29	885	−8.0	80	−82	16	0.91006	0.00344	:	:	32.7	32.7	4
21	30	935	−8.0	87	−80	18	0.90989	0.00348	:	:	33.4	33.3	4
22	31	944	−7.9	88	−80	19	0.91051	0.00349	:	:	33.5	33.5	4
23	52	945	−8.2	87	−80	18	0.90800	0.00348	:	:	33.5	33.5	4
24	54	1060	−7.8	87	−79	19	0.91200	0.00364	:	:	34.9	34.9	4
25	57	1250	−7.4	84	−80	18	0.91488	0.00389	:	:	36.9	36.9	3
26	58	1550	−6.3	75	−83	14	0.92499	0.00438	:	:	39.7	39.7	3
27	60	1640	−6.0	73	−85	13	0.92716	0.00455	:	:	40.6	40.6	3
28	62	1990	−4.2	71	−93	19	0.94311	0.00524	:	:	43.7	43.7	4
29	64	2140	−3.7	77	−98	25	0.94765	0.00553	:	:	45.1	45.1	4
30	66	2260	−3.2	88	−102	30	0.95225	0.00579	:	:	46.5	46.4	4
31	68	2390	−2.6	104	−107	35	0.95742	0.00608	:	:	48.0	47.9	4
—	**AerN**	1	50	—	—	—	—	—	—	—	—	—	—
0	B440	440	1.5	118	−33	36	1.01491	−0.00212	:	:	12.3	11.7	59
1	B500	500	1.5	90	−27	25	1.01532	−0.00164	:	:	9.4	8.9	45
2	B675	675	−0.6	75	−15	19	0.99434	−0.00130	:	:	8.0	7.6	34
3	B870	870	0.6	48	−11	11	1.00614	−0.00156	:	:	5.5	4.8	73
4	B1020	1020	−3.4	61	−16	11	0.96636	−0.00166	:	:	7.1	6.4	68
5	B1021	1021	−1.6	46	−12	10	0.98416	−0.00048	:	:	4.8	4.7	8
6	B1640	1640	4.1	102	−18	29	1.04089	−0.00107	:	:	10.0	9.9	16
—	**HiRIS**	0	4	—	—	—	—	—	—	—	—	—	—
0	BluGrn	501	−21.9	449	−61	44	:	:	:	:	:	:	:
1	Red	677	−29.8	407	−49	34	:	:	:	:	:	:	:
2	nIR	859	−35.7	332	−49	20	:	:	:	:	:	:	:
—	**OLI**	1	1080	—	—	—	—	—	—	—	—	—	—
0	Aer	443	3.8	41	−10	11	1.03644	−0.00090	:	:	4.3	4.0	28
1	Blu	482	1.3	22	−8	6	1.01231	−0.00035	:	:	2.2	2.1	8
2	Grn	562	0.8	33	−10	7	1.00594	−0.00022	:	:	3.2	3.2	2
3	Pan	590	1.4	27	−8	7	1.01309	−0.00020	:	:	2.6	2.6	2
4	Red	655	0.8	32	−10	7	1.00654	−0.00017	:	:	3.1	3.1	1

Table 7 (*Continued*).

1	2	3	4	5	6	7	8	9	10	11	12	13	14
			Calibration				Trend coefficient				Normalized SD		
Band index	Band name	Wave nm.	Mean	SD	Δ min	Δ max	c_0	$c_1 \vee \tau_1$	c_2	c_3	Cal	−Trend	Imp
5	NIR	865	1.9	28	−8	7	1.01840	−0.00034	:	:	2.8	2.8	6
6	Cir	1375	3.5	55	−14	12	1.03318	−0.00025	:	:	5.3	5.3	2
7	SW1	1610	−1.1	32	−9	7	0.98811	−0.00016	:	:	3.3	3.2	1
8	SW2	2200	−1.5	28	−8	6	0.98457	−0.00015	:	:	2.9	2.9	1
—	**OLIR**	4	72	—	—	—	—	—	—	—	—	—	—
0	Aer	443	4.3	15	−3	3	1.03570	0.25	0.01136	−0.0006	2.3	1.4	89
1	Blu	482	1.3	14	−3	2	1.01731	4.95	−0.00488	−0.0009	1.5	1.4	15
2	Grn	562	0.5	13	−3	2	1.00764	0.51	−0.00392	−0.0005	1.5	1.4	17
3	Pan	590	1.3	15	−3	3	1.01536	1.35	−0.00293	−0.0006	1.6	1.5	9
4	Red	655	0.6	13	−3	2	1.00846	0.73	−0.00353	−0.0005	1.5	1.4	13
5	NIR	865	1.8	13	−2	2	1.02086	1.84	−0.00284	−0.0007	1.5	1.3	17
6	Cir	1375	3.4	15	−3	3	1.03208	19.62	0.00148	−0.0002	1.6	1.5	7
7	SW1	1610	−1.2	13	−4	2	0.98918	1.28	−0.00121	−0.0003	1.4	1.4	5
8	SW2	2200	−1.5	15	−4	2	0.98490	500.00	0.00000	−0.0001	1.6	1.6	3
—	**HypM**	1	20	—	—	—	—	—	—	—	—	—	—
0	HM2	415	28.2	387	−125	56	1.44107	−0.01298	:	:	31.7	30.2	144
1	HM3	443	14.2	121	−23	23	1.19754	−0.00451	:	:	11.3	10.6	71
2	HM4	468	16.4	83	−14	11	1.19988	−0.00294	:	:	7.6	7.2	45
3	HM5	490	22.7	80	−14	10	1.25083	−0.00194	:	:	6.8	6.6	19
4	HM6	512	27.2	78	−14	10	1.29449	−0.00183	:	:	6.4	6.2	17
5	HM7	532	26.7	78	−14	10	1.28447	−0.00146	:	:	6.3	6.2	11
6	HM8	553	27.2	77	−14	10	1.29029	−0.00148	:	:	6.2	6.1	12
7	HM9	578	28.0	80	−15	10	1.29949	−0.00163	:	:	6.4	6.3	13
8	HM10	613	30.1	88	−15	12	1.32288	−0.00176	:	:	7.0	6.8	14
9	HM11	648	29.8	85	−15	11	1.31520	−0.00140	:	:	6.7	6.6	9
10	HM12	666	26.0	79	−15	10	1.26986	−0.00079	:	:	6.4	6.3	3
11	HM13	680	26.8	80	−15	10	1.28327	−0.00129	:	:	6.4	6.4	9
12	HM14	704	27.2	83	−15	11	1.29328	−0.00177	:	:	6.7	6.6	15
13	HM15	730	24.6	82	−15	11	1.27272	−0.00216	:	:	6.8	6.6	23
14	HM16	750	24.5	84	−16	11	1.27808	−0.00274	:	:	7.2	6.8	36
15	HM17	775	25.2	91	−17	12	1.29638	−0.00362	:	:	7.8	7.3	57
16	HM18	850	28.1	82	−16	11	1.33239	−0.00425	:	:	7.3	6.5	83
17	HM19	870	26.2	84	−16	11	1.32864	−0.00543	:	:	8.0	6.7	131

Table 7 (*Continued*).

1	2	3	4	5	6	7	8	9	10	11	12	13	14
			Calibration				Trend coefficient				Normalized SD		
Band index	Band name	Wave nm.	Mean	SD	Δ min	Δ max	c_0	$c_1 \vee \tau_1$	c_2	c_3	Cal	−Trend	Imp
18	HM20	915	18.4	101	−24	14	1.27893	−0.00779	:	:	10.9	8.6	230
19	HM21	1060	20.8	95	−17	21	1.26311	−0.00455	:	:	8.8	7.9	89
20	HM22	1245	17.4	80	−17	12	1.22406	−0.00410	:	:	7.7	6.8	86
21	HM23	1383	23.9	104	−23	18	1.29797	−0.00483	:	:	9.3	8.4	87
22	HM24	1608	19.0	93	−17	16	1.20704	−0.00144	:	:	7.9	7.8	10
23	HM25	2160	23.2	111	−21	16	1.27287	−0.00336	:	:	9.5	9.1	41
24	HM26	2255	20.5	84	−15	14	1.23298	−0.00232	:	:	7.3	7.0	27
25	HM27	2383	28.0	109	−18	22	1.26865	0.00089	:	:	8.6	8.5	3
—	**MODT**	1	993	—	—	—	—	—	—	—	—	—	—
0	b8	412	1.2	86	−22	31	1.01283	0.00014	:	:	8.6	8.5	3
1	b9	443	1.4	66	−20	22	1.01513	−0.00002	:	:	6.5	6.5	0
2	b3	469	1.3	79	−25	32	1.01425	0.00034	:	:	8.1	7.8	21
3	b10	488	1.7	47	−14	12	1.01751	−0.00025	:	:	4.8	4.6	20
4	b11	531	−0.1	38	−12	12	0.99962	−0.00003	:	:	3.8	3.8	0
5	b12	551	1.1	39	−15	9	1.01185	0.00003	:	:	3.9	3.9	0
6	b4	555	−0.5	52	−17	13	0.99552	0.00002	:	:	5.3	5.3	0
7	b1	645	−2.2	88	−22	23	0.97828	0.00129	:	:	11.5	9.0	251
8	b13	666	0.4	41	−11	12	1.00509	0.00011	:	:	4.2	4.1	4
9	b14	678	−0.2	52	−15	16	0.99868	0.00003	:	:	5.2	5.2	0
10	b15	748	0.7	50	−18	13	1.00799	0.00009	:	:	5.0	5.0	2
11	b2	858	−0.4	83	−19	26	0.99681	0.00146	:	:	11.5	8.4	317
12	b16	868	1.4	41	−13	13	1.01513	−0.00003	:	:	4.1	4.1	0
13	b17	905	4.2	42	−11	12	1.04313	−0.00004	:	:	4.0	4.0	0
14	b18	936	3.4	47	−12	13	1.03453	0.00001	:	:	4.6	4.6	0
15	b19	940	4.1	39	−10	12	1.04130	−0.00005	:	:	3.8	3.8	1
16	b5	1240	30.3	321	−86	159	1.30417	0.00214	:	:	26.1	24.7	146
17	b26	1375	9.5	150	−42	75	1.09575	0.00053	:	:	13.9	13.7	23
18	b6	1640	9.8	117	−47	66	1.09927	0.00053	:	:	11.0	10.7	30
19	b7	2130	−4.3	151	−39	64	0.95749	0.00087	:	:	16.5	15.8	73
—	**MODA**	1	743	—	—	—	—	—	—	—	—	—	—
0	b8	412	3.1	74	−24	22	1.03146	−0.00041	:	:	7.5	7.3	24
1	b9	443	2.0	42	−13	12	1.01980	−0.00028	:	:	4.4	4.2	20
2	b3	469	0.3	47	−15	11	1.00262	−0.00010	:	:	4.8	4.7	2

Table 7 (*Continued*).

1	2	3	4	5	6	7	8	9	10	11	12	13	14
			Calibration				Trend coefficient				Normalized SD		
Band index	Band name	Wave nm.	Mean	SD	Δ min	Δ max	c_0	$c_1 \vee \tau_1$	c_2	c_3	Cal	−Trend	Imp
3	b10	488	1.2	33	−10	11	1.01177	−0.00014	:	:	3.4	3.4	7
4	b11	531	−1.2	28	−10	8	0.98851	−0.00014	:	:	3.0	2.9	7
5	b12	551	0.3	31	−11	6	1.00321	−0.00013	:	:	3.2	3.1	6
6	b4	555	−1.6	32	−12	7	0.98426	−0.00005	:	:	3.4	3.3	1
7	b1	645	−1.3	55	−17	13	0.98655	0.00054	:	:	6.2	5.6	57
8	b13	666	1.1	52	−13	15	1.01119	−0.00035	:	:	5.5	5.2	25
9	b14	678	1.2	61	−14	17	1.01213	−0.00033	:	:	6.2	6.1	20
10	b15	748	1.2	159	−53	29	1.01271	−0.00046	:	:	15.9	15.7	14
11	b2	858	−0.1	51	−14	12	0.99920	0.00116	:	:	7.4	5.1	233
12	b16	868	−1.1	359	−96	52	0.98913	−0.00036	:	:	36.4	36.4	4
13	b17	905	3.7	31	−10	12	1.03670	−0.00009	:	:	3.0	3.0	3
14	b18	936	3.3	35	−12	13	1.03330	−0.00004	:	:	3.5	3.5	0
15	b19	940	3.7	30	−9	12	1.03756	−0.00005	:	:	2.9	2.9	1
16	b5	1240	15.3	294	−69	69	1.15346	−0.00105	:	:	25.9	25.5	36
17	b26	1375	4.3	143	−32	21	1.04324	−0.00016	:	:	13.8	13.8	2
18	b7	2130	−3.0	74	−18	21	0.96995	−0.00008	:	:	7.7	7.7	1
—	**SeaW**	4	204	—	—	—	—	—	—	—	—	—	—
0	1	412	−2.1	67	−20	28	0.96506	10.21	0.01523	0.0010	6.9	6.9	5
1	2	443	−2.2	67	−21	28	0.97577	5.55	0.00209	0.0003	6.9	6.9	3
2	3	490	−3.1	68	−18	30	0.98932	232.10	−0.02034	0.0002	7.1	7.1	8
3	4	510	−3.9	69	−18	31	0.98449	140.01	−0.02308	0.0001	7.3	7.2	9
4	5	555	−4.8	72	−19	33	0.97685	26.90	−0.02457	−0.0003	7.7	7.6	11
5	6	670	−5.2	74	−19	33	0.97798	17.81	−0.03010	−0.0007	8.0	7.8	15
6	7	765	−3.6	75	−18	31	0.99452	15.82	−0.03073	−0.0008	8.0	7.8	20
7	8	865	−5.3	69	−21	28	0.95580	−804.76	−0.00924	−0.0000	7.3	7.3	1
—	**VIIRS**	4	71	—	—	—	—	—	—	—	—	—	—
0	M1	421	−21.3	13	−6	4	0.77805	1.74	0.01185	−0.0052	19.0	1.7	1731
1	M2	446	6.9	10	−2	2	1.06656	1.06	0.00592	−0.0035	8.6	0.9	775
2	M3	489	11.4	26	−14	2	1.09614	402.94	0.01779	−0.0039	8.9	2.3	653
3	M4	552	10.8	13	−2	3	1.09489	9.90	0.01332	−0.0030	8.7	1.1	762
4	I1	638	3.9	19	−4	4	0.99893	0.49	0.06211	−0.0063	20.9	1.8	1906
5	M5	671	3.6	16	−3	2	0.97414	0.46	0.09531	−0.0079	28.2	1.5	2663
6	M6	745	−5.3	23	−4	4	0.82935	0.43	0.18470	−0.0114	53.7	2.4	5126

Table 7 (*Continued*).

1	2	3	4	5	6	7	8	9	10	11	12	13	14
			Calibration				Trend coefficient				Normalized SD		
Band index	Band name	Wave nm.	Mean	SD	Δ min	Δ max	c_0	$c_1 \vee \tau_1$	c_2	c_3	Cal	−Trend	Imp
7	I2	861	−7.0	40	−8	8	0.72892	0.42	0.32007	−0.0164	97.2	4.3	9283
8	M7	862	−6.9	40	−7	8	0.72832	0.41	0.32383	−0.0160	96.0	4.3	9166
9	M8	1241	−8.7	33	−9	6	0.73163	0.44	0.27973	−0.0153	80.1	3.7	7649
10	M9	1375	−3.1	29	−8	4	0.83374	0.49	0.20174	−0.0132	52.2	3.0	4921
11	I3	1601	−1.4	26	−7	4	0.89505	0.43	0.14266	−0.0092	37.8	2.7	3518
12	M10	1602	−2.2	25	−8	3	0.88750	0.44	0.14024	−0.0091	35.2	2.6	3254
13	M11	2257	3.6	17	−5	2	1.01018	0.47	0.03992	−0.0030	9.8	1.7	818
—	**VIIRN**	1	28	—	—	—	—	—	—	—	—	—	—
0	M1	421	17.5	14	−2	2	1.17464	−0.00012	:	:	1.2	1.2	0
1	M2	446	12.9	10	−1	2	1.12898	−0.00107	:	:	1.3	0.9	43
2	M3	489	12.7	8	−1	1	1.12686	−0.00093	:	:	1.1	0.7	40
3	M4	552	13.5	7	−1	1	1.13504	−0.00109	:	:	1.2	0.6	53
4	I1	638	10.5	10	−2	2	1.10496	−0.00136	:	:	1.6	1.0	62
5	M5	671	14.6	8	−1	2	1.14575	−0.00080	:	:	1.0	0.7	30
6	M6	745	12.9	10	−1	1	1.12901	−0.00059	:	:	1.0	0.9	15
7	I2	861	11.7	12	−1	2	1.11644	−0.00019	:	:	1.1	1.1	1
8	M7	862	14.0	19	−3	2	1.13959	−0.00006	:	:	1.7	1.7	0
9	M8	1241	1.9	12	−2	1	1.01850	−0.00008	:	:	1.2	1.2	0
10	M9	1375	−1.3	15	−2	2	0.98629	0.00034	:	:	1.6	1.6	4
11	I3	1601	−0.5	16	−2	3	0.99443	0.00001	:	:	1.7	1.7	0
12	M10	1602	−2.5	13	−3	1	0.97495	−0.00008	:	:	1.3	1.3	0
13	M11	2257	4.7	12	−2	2	1.04671	−0.00038	:	:	1.3	1.2	5
—	**PleA**	1	141	—	—	—	—	—	—	—	—	—	—
0	Blue	490	−0.8	50	−12	16	0.99157	−0.00125	:	:	11.1	10.8	24
1	Green	560	2.4	76	−29	20	1.02370	−0.00286	:	:	13.1	12.2	96
2	Red	650	0.4	61	−49	9	1.00282	0.00056	:	:	12.4	12.3	2
3	Pan	655	−0.2	62	−37	10	0.99976	−0.00142	:	:	28.8	28.6	19
4	NIR	840	1.9	50	−44	8	1.01820	0.00132	:	:	13.2	13.0	15
—	**PleB**	4	339	—	—	—	—	—	—	—	—	—	—
0	Blue	490	−0.2	43	−33	14	0.52231	11.70	0.47284	0.0318	41.0	40.8	13
1	Green	560	1.9	40	−21	8	0.52922	16.87	0.48537	0.0236	42.3	42.2	8
2	Red	650	1.4	34	−22	8	0.51132	−46.63	0.49567	−0.0100	44.5	44.5	−2
3	Pan	655	0.2	48	−16	9	0.50892	144.60	0.48729	0.0038	44.1	44.1	−1
4	NIR	840	2.5	42	−18	13	0.50242	76.19	0.51649	0.0076	47.3	47.3	−1

Table 7 (*Continued*).

1	2	3	4	5	6	7	8	9	10	11	12	13	14
			Calibration				Trend coefficient				Normalized SD		
Band index	Band name	Wave nm.	Mean	SD	Δ min	Δ max	c_0	$c_1 \vee \tau_1$	c_2	c_3	Cal	−Trend	Imp
—	**GS8**	2	44	—	—	—	—	—	—	—	—	—	—
0	Pan	635	−28.4	179	−49	30	0.73719	24.34	:	:	98.9	25.1	7379
—	**GS9**	1	9	—	—	—	—	—	—	—	—	—	—
0	Pan	638	−16.7	340	−51	39	0.84159	−0.01461	:	:	43.0	40.9	208
—	**GS10**	3	49	—	—	—	—	—	—	—	—	—	—
0	Pan	651	−5.9	229	−64	61	0.59258	3.66	0.49688	:	147.2	24.4	12279
—	**GS11**	1	77	—	—	—	—	—	—	—	—	—	—
0	Pan	658	−15.2	150	−54	52	1.03576	−0.02952	:	:	54.1	17.7	3640
—	**GS12**	3	49	—	—	—	—	—	—	—	—	—	—
0	Pan	651	−11.7	150	−50	39	0.63111	4.18	0.38176	:	74.6	17.0	5761
—	**GS13**	1	47	—	—	—	—	—	—	—	—	—	—
0	Pan	627	−16.7	179	−54	42	0.94622	−0.02705	:	:	35.8	21.6	1418
—	**GS15**	1	28	—	—	—	—	—	—	—	—	—	—
0	Pan	625	−18.5	136	−29	37	0.90315	−0.04376	:	:	32.5	20.1	1237
—	**SEV1**	1	1209	—	—	—	—	—	—	—	—	—	—
0	VIS006	635	−7.0	110	−33	28	0.91468	−0.00064	:	:	75.1	75.0	6
1	HRVIS	750	−5.0	202	−17	39	0.91189	−0.00375	:	:	191.7	190.6	107
2	VIS008	810	−4.0	117	−34	30	0.93352	−0.00051	:	:	112.8	112.8	5
3	NIR016	1640	5.8	146	−61	50	1.03312	0.00030	:	:	109.9	109.9	0
—	**SEV2**	1	1152	—	—	—	—	—	—	—	—	—	—
0	VIS006	635	−6.5	121	−42	30	0.92446	−0.00164	:	:	80.7	80.4	33
1	HRVIS	750	−5.6	830	−779	43	0.88007	0.00133	:	:	185.6	185.7	−12
2	VIS008	810	−3.5	108	−45	26	0.94527	−0.00043	:	:	77.4	77.4	4
3	NIR016	1640	6.4	154	−76	43	1.03075	0.00145	:	:	98.3	98.3	4
—	**SEV3**	1	556	—	—	—	—	—	—	—	—	—	—
0	VIS006	635	−8.4	114	−41	32	0.88916	0.00025	:	:	77.8	77.8	−1
1	HRVIS	750	−5.4	202	−12	32	0.86576	0.00448	:	:	187.2	187.0	25
2	VIS008	810	−3.4	121	−49	29	0.94402	−0.00067	:	:	78.2	78.2	5
3	NIR016	1640	6.4	130	−75	34	1.04214	0.00162	:	:	80.4	80.4	2
—	**SEV4**	1	199	—	—	—	—	—	—	—	—	—	—
0	VIS006	635	−7.7	122	−28	21	0.88734	0.00419	:	:	85.0	84.9	5
1	HRVIS	750	−9.4	687	−89	71	0.84669	0.01821	:	:	118.6	113.3	532
2	VIS008	810	−2.8	206	−59	26	0.94692	0.00436	:	:	54.3	53.9	38
3	NIR016	1640	7.2	232	−64	34	1.04134	0.00738	:	:	73.1	72.4	72

Table 7 (*Continued*).

1	2	3	4	5	6	7	8	9	10	11	12	13	14
			Calibration				Trend coefficient				Normalized SD		
Band index	Band name	Wave nm.	Mean	SD	Δ min	Δ max	c_0	$c_1 \vee \tau_1$	c_2	c_3	Cal	−Trend	Imp
—	**ABI16**	1	115	—	—	—	—	—	—	—	—	—	—
0	B01	470	2.9	117	−18	54	1.00235	0.01025	:	:	12.0	11.4	59
1	B02	640	−0.5	66	−14	14	0.99570	−0.00045	:	:	6.7	6.7	0
2	B03	865	1.8	38	−7	12	1.01684	0.00014	:	:	3.7	3.7	0
3	B04	1378	1.1	48	−8	13	1.00827	0.00080	:	:	4.8	4.8	1
4	B05	1610	2.3	68	−13	16	1.01300	0.00341	:	:	6.8	6.7	11
5	B06	2250	1.4	90	−17	20	0.99958	0.00521	:	:	9.1	8.9	20
—	**ABI17**	1	121	—	—	—	—	—	—	—	—	—	—
0	B01	470	4.2	169	−21	62	1.02900	0.01036	:	:	16.6	16.2	41
1	B02	640	3.9	224	−208	32	1.02798	0.00851	:	:	21.8	21.6	21
2	B03	865	2.5	86	−18	22	1.00872	0.01314	:	:	9.6	8.4	117
3	B04	1378	5.5	89	−15	23	1.05313	0.00129	:	:	8.5	8.5	1
4	B05	1610	6.6	100	−16	27	1.05741	0.00652	:	:	9.7	9.4	26
5	B06	2250	3.1	111	−20	27	1.02469	0.00515	:	:	10.9	10.8	16
—	**GIRO**	0	1610	—	—	—	—	—	—	—	—	—	—
0	16	345	−1.3	113	−46	13	:	:	:	:	:	:	:
1	17	355	−1.4	100	−41	13	:	:	:	:	:	:	:
2	18	405	−3.1	68	−30	10	:	:	:	:	:	:	:
3	2	412	−3.1	67	−32	10	:	:	:	:	:	:	:
4	19	415	−3.2	64	−30	10	:	:	:	:	:	:	:
5	4	443	−3.9	49	−24	10	:	:	:	:	:	:	:
6	20	465	−4.7	52	−26	11	:	:	:	:	:	:	:
7	21	475	−4.8	46	−24	11	:	:	:	:	:	:	:
8	6	488	−5.0	45	−23	12	:	:	:	:	:	:	:
9	22	545	−6.2	54	−26	8	:	:	:	:	:	:	:
10	8	551	−6.0	49	−25	8	:	:	:	:	:	:	:
11	23	555	−6.4	55	−28	8	:	:	:	:	:	:	:
12	10	667	−7.7	49	−24	8	:	:	:	:	:	:	:
13	24	695	−7.8	45	−23	8	:	:	:	:	:	:	:
14	25	705	−7.9	48	−23	9	:	:	:	:	:	:	:
15	12	748	−8.1	48	−24	7	:	:	:	:	:	:	:
16	26	765	−8.1	42	−22	16	:	:	:	:	:	:	:

Table 7 (*Continued*).

1	2	3	4	5	6	7	8	9	10	11	12	13	14
			Calibration				Trend coefficient				Normalized SD		
Band index	Band name	Wave nm.	Mean	SD	Δ min	Δ max	c_0	$c_1 \vee \tau_1$	c_2	c_3	Cal	−Trend	Imp
17	27	775	−8.3	45	−24	9	:	:	:	:	:	:	:
18	14	869	−8.9	63	−27	10	:	:	:	:	:	:	:
19	28	875	−8.9	67	−30	10	:	:	:	:	:	:	:
20	29	885	−9.0	70	−31	10	:	:	:	:	:	:	:
21	30	935	−9.2	83	−39	14	:	:	:	:	:	:	:
22	31	944	−9.9	166	−50	25	:	:	:	:	:	:	:
23	52	945	−9.8	159	−49	24	:	:	:	:	:	:	:
24	54	1060	−9.6	167	−60	20	:	:	:	:	:	:	:
25	57	1250	−8.3	106	−36	14	:	:	:	:	:	:	:
26	58	1550	−6.6	68	−25	12	:	:	:	:	:	:	:
27	60	1640	−5.6	60	−21	12	:	:	:	:	:	:	:
28	62	1990	−3.4	42	−21	10	:	:	:	:	:	:	:
29	64	2140	−3.0	191	−48	52	:	:	:	:	:	:	:
30	66	2260	−1.6	58	−23	16	:	:	:	:	:	:	:
31	68	2390	−0.3	72	−16	17	:	:	:	:	:	:	:
—	**LIIMO**	0	1610	—	—	—	—	—	—	—	—	—	—
0	band_1	440	−3.1	102	−22	28	:	:	:	:	:	:	:
1	band_2	500	−3.3	89	−20	27	:	:	:	:	:	:	:
2	band_3	675	−4.9	81	−19	24	:	:	:	:	:	:	:
3	band_4	870	−6.1	94	−21	25	:	:	:	:	:	:	:
4	band_5	1020	−6.1	110	−24	26	:	:	:	:	:	:	:
5	band_6	1640	−6.9	88	−22	23	:	:	:	:	:	:	:
—	**SLIMO**	0	54	—	—	—	—	—	—	—	—	—	—
0	G1	442	−0.0	19	−6	5	:	:	:	:	:	:	:
1	G2	550	0.1	20	−6	4	:	:	:	:	:	:	:
2	G3	670	0.1	21	−7	4	:	:	:	:	:	:	:
3	G4	765	0.2	22	−7	5	:	:	:	:	:	:	:
4	G5	870	0.2	23	−7	5	:	:	:	:	:	:	:
5	G6	1380	0.1	25	−7	6	:	:	:	:	:	:	:
6	G7	1640	0.1	26	−8	6	:	:	:	:	:	:	:
7	G8	2350	−0.1	27	−8	7	:	:	:	:	:	:	:

Table 8 Instrument dates, grouped by type. Date of launch and date range covered by data on hand.

		Launch	First	Last
Instrument	Acronym	Dates	Observation	Observation
—	—	LEO	—	—
SeaWIFS	SeaW	September 20, 1997	November 14, 1997	November 22, 2010
EO1-Hyperion	HypM	November 21, 2000	February 26, 2013	February 23, 2016
Terra-MODIS	MODT	December 18, 1999	March 24, 2000	February 23, 1999
Aqua-MODIS	MODA	May 04, 2002	June 20, 2002	February 15, 2019
Suomi-VIIRS	VIIRS	October 28, 2011	January 04, 2012	March 05, 2020
NOAA-20-VIIRS	VIIRN	November 18, 2017	December 29, 2017	March 24, 2021
Landsat-8-OLI	OLI	February 11, 2013	March 26, 2013	January 21, 2019
PLEIADES-A	PleA	December 17, 2011	January 02, 2012	April 07, 2017
PLEIADES-B	PleB	December 02, 2012	February 17, 2013	April 07, 2017
—	—	GEO	—	—
GOES-8	GS8	April 13, 1994	January 08, 1995	February 20, 2003
GOES-9	GS9	May 23, 1995	December 12, 1995	April 12, 1998
GOES-10	GS10	April 25, 1997	August 09, 1998	June 06, 2006
GOES-11	GS11	May 03, 2000	September 08, 2006	December 04, 2011
GOES-12	GS12	July 23, 2001	April 14, 2003	March 02, 2010
GOES-13	GS13	May 24, 2006	July 30, 2010	November 14, 2013
GOES-15	GS15	February 05, 2010	March 06, 2012	November 14, 2013
MSG-1-SEVIRI	SEV1	August 28, 2002	November 04, 2003	December 31, 2019
MSG-2-SEVIRI	SEV2	December 22, 2005	July 04, 2006	December 31, 2019
MSG-3-SEVIRI	SEV3	July 5, 2012	January 01, 2013	December 19, 2019
MSG-4-SEVIRI	SEV4	July 05, 2015	August 29, 2015	December 21, 2019
GOES-16-ABI	ABI16	November 03, 2016	May 14, 2019	July 10, 2020
GOES-17-ABI	ABI17	March 01, 2018	May 14, 2019	June 11, 2020
—	—	Other	—	—
Observ.@2148m	ROLOG	February 29, 1996	July 03, 1998	December 17, 2000
Observ.@2367m	NIST	November 30, 2012	November 30, 2012	November 30, 2012
Observ.@3402m	AerN	February 26, 2016	March 27, 2016	June 27, 2021
HiRISE-Mars	HiRIS	August 12, 2002	November 20, 2016	November 20, 2016

Acknowledgments

The author is grateful for the support of many individuals through the time of this work and expresses his appreciation to them. His family, for stupendous tolerance. Tom Stone for assistance in acquiring some of the datasets and for many discussions about the development of the SLIMED model and lunar calibration in general. Lawrence Ong for early support and

encouragement in development of the SLIM system and for OLI data and Hyperion lunar images. Steve Brown and Sebastien Wagner for very helpful reviews of the manuscript. R.E. Eplee Jr., for SeaWiFS data and belief in lunar calibration for 20 years. Brian Markham and NASA-GSFC for contract support for improved OLI lunar calibration that led to this work. Greg Kopp for help in selecting and structuring data on solar total irradiance and spectral variation. X. (Jack) Xiong for providing the lunar data for Modis-Terra and -Aqua, and both VIRRS. Aime Meygret for PLEIADES data. Sebastien Wagner for SEVIRI data. Fangfang Yu for ABI data. Ilya Slutsker for AeroNet Mauna Loa data. Ken Herkenhoff for HiRISE data. P. Lucey for the LOLA reflectance data. N. Piacentine of ASU for computer system administration. The Planetary Data System, cartography section at the USGS Astrogeology group for production of lunar maps. Sir David Attenborough, for inspiration. The author declares no conflict of interest. This work had no funding.

Data, Materials, and Code Availability

The Base and V1 models can be implemented from information in this article. A full set of IDL code to do an instrument calibration using a SLIMED model is available by contacting the author. Hopefully, some organization will convert this to a common computer language. The JPL DE430 ephemeris and FORTRAN code to run that is also required. Source code for all IDL routines called at any level by the SLIM system is archived at an academic institution and currently available only to two younger colleagues. It includes 252 routines, about 38,000 lines of high-level executable code, and totals about 4 Mb. Also archived there are all nonembargoed data files and SLIMED output files, descriptions of all file contents, and a user guide to running the SLIM system, about 400 Mb. This is intended to be transferred to a US government institution. Public access is unresolved.

References

1. H. H. Kieffer, "Photometric stability of the lunar surface," *Icarus* **130**, 323–327 (1997).
2. H. H. Kieffer and R. L. Wildey, "Absolute calibration of Landsat instruments using the Moon," *Photogramm. Eng. Remote Sens.* **51**, 1391–1393 (1985).
3. H. H. Kieffer and T. C. Stone, "The spectral irradiance of the Moon," *Astron. J.* **129**, 2887–2901 (2005).
4. B. Viticchiè et al., "Lunar calibration of MSG/SEVIRI solar channels," in *Proc. AMS-EUMETSAT Meteorol. Satell. Conf.*, Vienna (2013).
5. S. C. Wagner et al., "A summary of the joint GSICS – CEOS/IVOS lunar calibration workshop: moving towards intercalibration using the Moon as a transfer target," *Proc. SPIE* **9639**, 96390Z (2015).
6. T. C. Stone and H. H. Kieffer, "Assessment of uncertainty in ROLO lunar irradiance for on-orbit calibration," *Proc. SPIE* **5542**, 300–310 (2004).
7. T. C. Stone, "Radiometric calibration stability and inter-calibration of solar-band instruments in orbit using the moon," *Proc. SPIE* **7081**, 70810X (2008).
8. Y. I. Velikodsky et al., "New Earth-based absolute photometry of the Moon," *Icarus* **214**, 30–45 (2011).
9. Y. G. Shkuratov et al., "Absolute calibration of the clementine UV-VIS data: comparison with ground-based observation of the Moon," *Solar Syst. Res.* **35**, 29–34 (2001).
10. S. D. Miller and R. E. Turner, "A dynamic lunar spectral irradiance data set for NPOESS/VIIRS day/night band nighttime environmental applications," *IEEE Trans. Geosci. Remote Sens.* **47**, 2316–2329 (2009).
11. Y. Wang et al., "Comparison of the lunar models using the hyper-spectral imager observations in Lijiang, China," *Remote Sens.* **12**(11), 1878 (2020).
12. S. Taylor et al., "LIME: the Lunar Irradiance Model of the European Space Agency," in *EGU General Assembly 2021, 19–30 Apr 2021*, p. 10066 (2021).
13. T. C. Stone et al., "The Moon as a climate-quality radiometric calibration reference," *Remote Sens.* **12**(11), 1837 (2020).

14. D. E. Wilhelms, "The geologic history of the Moon," U.S. Geological Survey Professional Paper 1348 (1987).
15. H. Hiesinger et al., "Ages and stratigraphy of mare basalts in Oceanus Procellarum, Mare Nubium, Mare Cognitum, and Mare Insularum," *J. Geophys. Res: Planets* **108**(E7), 1–27 (2003).
16. B. W. Hapke, *Theory of Reflectance and Emittance Spectroscopy*, 2nd ed., Cambridge University Press, Cambridge (2012).
17. Y. I. Velikodsky et al., "Opposition effect of the Moon from LROC WAC data," *Icarus* **275**, 1–15 (2016).
18. J. L. Hinrichs and P. G. Lucey, "Temperature-dependent near-infrared spectral properties of minerals, meteorites, and lunar soil," *Icarus* **155**, 169–180 (2002).
19. B. Lyot, "Polarization of moonlight and selected lunar regions," *Ann. Obs. Meudon* **8**, 1–56 (1929).
20. A. Dollfus and E. Bowell, "Polarimetric properties of the lunar surface and its interpretation. Part I. Telescopic observations," *Astron. Astrophys.* **10**, 29 (1971).
21. Y. Shkuratov et al., "Optical measurements of the moon as a tool to study its surface," *Planet. Space Sci.* **59**(13), 1326–1371 (2011).
22. C. Pieters, "Strength of mineral absorption features in the transmitted component of near-infrared reflected light: first results from RELAB," *J. Geophys. Res.* **88**(B11), 9534–9544 (1983).
23. C. M. Pieters, "The Moon as a calibration standard enabled by lunar samples," 1999, http://www.planetary.brown.edu/pds/AP62231.html In New Views of the Moon II: Understanding the Moon through the Integration of Diverse Datasets, Workshop held in Flagstaff, abstract 8025.
24. L. A. Taylor et al., "Lunar mare soils: space weathering and the major effects of surface-correlated nanophase Fe," *J. Geophys. Res.: Planets* **106**(E11), 27985–27999 (2001).
25. M. Abramowitz and I. Stegun, *Handbook of Mathematical Functions*, Dover, New York (1964).
26. E. M. Eliason et al., "Multispectral mapping of the moon by clementine," in *Workshop on New Views of the Moon: Integrated Remotely Sensed, Geophysical, and Sample Datasets*, Lunar and Planetary Institute, Flagstaff, Arizona, pp. 26–27 (1998).
27. P. Lucey et al., "The global albedo of the Moon at 1064 nm from LOLA," *J. Geophys. Res. Planets* **119**, 1665–1679 (2014).
28. M. Lemelin et al., "Improved calibration of reflectance data from the LRO Lunar Orbiter Laser Altimeter (LOLA) and implications for space weathering," *Icarus* **273**, 315–328 (2016).
29. A. S. McEwen, "A precise lunar photometric function," *Lunar Planet. Sci.* **27**, 841–842 (1996).
30. A. McEwen et al., "Summary of radiometric calibration and photometric normalization steps for the Clementine UVVIS images," *Lunar Planet. Sci.* **29**, 1466–1467 (1998).
31. B. J. Buratti et al., "A wavelength-dependent visible and infrared spectrophotometric function for the Moon based on ROLO data," *J. Geophs. Res. (Planets)* **116**, E00G03 (2011).
32. M. D. Hicks et al., "A photometric function for analysis of lunar images in the visual and infrared based on moon mineralogy mapper observations," *J. Geophys. Res.: Planets* **116**(E6), E00G15 (2011).
33. Y. Yokota et al., "Lunar photometric properties at wavelengths acquired by SELENE Spectral Profiler and their dependency on local albedo and latitudinal zones," *Icarus* **215**, 639–660 (2011).
34. O. Coddington et al., "The TSIS-1 hybrid solar reference spectrum," *Geophys. Res. Lett.* **48**, 777–707 (2021).
35. D. de Wit et al., "Methodology to create a new total solar irradiance record: making a composite out of multiple data records," *Geophys. Res. Lett* **44**, 1196–1203 (2017).
36. G. Kopp, "TSI composite using methodology of Dudok de Wit et al. 2017," 2020, https://spot.colorado.edu/~koppg/TSI/TSI_Composite-SIST.txt.
37. E. Richard, G. Kopp, and P. Pilewskie, "Implementation of solar irradiance measurements on the International Space Station (ISS): the TSIS-1 mission of total and spectral solar

irradiance observational continuity," in *Space Weather Workshop, April 16-20*, Westminster, CO (2018).
38. G. Kopp, "TSIS TIM level 3 total solar irradiance 6-hour means, version 03, 6 hour cadence," 2021, http://lasp.colorado.edu/data/tsis/tsi_data/tsis_tsi_L3_c06h_latest.txt.
39. C. Cramer et al., "Precise measurement of lunar spectral irradiance at visible wavelengths," *J. Res. Natl. Inst. Standards and Tech.* **118**, 396–402 (2013).
40. W. Folkner et al., "The planetary and lunar ephemeris DE 430 and 431," 2014, https://ipnpr.jpl.nasa.gov/progress_report/42-196/196C.pdf.
41. X. Xiong et al., "MODIS and VIIRS lunar observations and applications," *Proc. SPIE* **8889**, 88890V (2013).
42. X. Xiong et al., "Comparison of MODIS and PLEIADES Lunar observations," *Proc. SPIE* **9241**, 924111 (2014).
43. X. Xiong et al., "Sixteen years of Terra MODIS on-orbit operation, calibration, and performance," *Proc. SPIE* **10000**, 100000V (2016).
44. R. E. Eplee et al., "On-orbit calibration of SeaWiFS," *Appl. Opt.* **51**, 8702–8730 (2012).
45. B. Markham et al., "Landsat-8 operational land imager radiometric calibration and stability," *Remote Sens.* **6**, 12275–12308 (2014).
46. X. Xiong et al., "Assessment of S-NPP VIIRS on-orbit radiometric calibration and performance," *Remote Sens.* **8**(2), 84 (2016).
47. J. Sun, X. Xiong, and J. Butler, "NPP VIIRS on-orbit calibration and characterization using the moon," *Proc. SPIE* **8510**, 85101I (2012).
48. X. Xiong et al., "Lunar Calibration and Performance for S-NPP VIIRS Reflective Solar Bands," *IEEE Trans. Geosci. Remote Sens.* **54**(2), 1052–1061 (2016).
49. T. Choi, X. Shao, and C. Cao, "On-orbit radiometric calibration of Suomi NPP VIIRS reflective solar bands using the Moon and solar diffuser," *Appl. Opt.* **57**, 9533–9542 (2018).
50. R. E. Eplee, Jr. et al., "The NASA OBPG 2020 on-orbit calibration of SNPP VIIRS for ocean color applications," *Proc. SPIE* **11127**, 111271A (2019).
51. S. Lacherade et al., "POLO: a unique dataset to derive the phase angle dependence of the Moon irradiance," *Proc. SPIE* **9241**, 924112 (2014).
52. M. A. Folkman et al., "EO-1/Hyperion hyperspectral imager design, development, characterization, and calibration," *Proc. SPIE* **4151**, 40–51 (2001).
53. J. McCorkel, K. Thome, and L. Ong, "Vicarious calibration of EO-1 hyperion," *IEEE J. Sel. Top. Appl. Earth Obs. Remote Sens.* **6**(2), 400–407 (2013).
54. C. Tranquilli et al., "Meteosat SEVIRI performance characterisation and calibration with dedicated Moon/Sun/deep-space scans," in *SpaceOps Conf. 16-20 May 2016*, Daejeon, American Institute of Aeronautics and Astronautics (2016).
55. T. C. Stone, H. H. Kieffer, and I. F. Grant, "Potential for calibration of geostationary meteorological imagers using the Moon," *Proc. SPIE* **5882**, 58820P (2005).

Hugh H. Kieffer was a professor at UCLA (1968–1978) then research geophysicist with the USGS (1978–2003). He received his BS degree in geology and PhD in planetary science from the Caltech. He is a fellow of the AGU. He has been in involved every US Mars mission except Sojourner from 1969 to 2018 as an investigator (PI on Viking) or Standing Review Board member, and is lead author of the book "Mars." He has promoted lunar calibration since 1985. He initiated the Global Land Ice Measurements from Space (GLIMS) organization in 1994.